Radio Source Signal Localization Methods and Hardware Simulation

by

Patrick Carter

A thesis submitted to the Graduate Faculty of
Auburn University
in partial fulfillment of the
requirements for the Degree of
Master of Science

Auburn, Alabama
May 6, 2023

Keywords: GPS, Navigation, Estimation, Localization, CRPA, Direction Finding

Approved by

Scott Martin, Chair, Associate Professor of Electrical and Computer Engineering
David Bevly, Ginn Distinguished Professor of Electrical and Computer Engineering
Lloyd Riggs, Professor of Electrical and Computer Engineering

Abstract

This thesis identifies and derives several methods of transmitter localization as well as collects several pre-existing algorithms and adapts them to the use of passive GPS interference localization. Due to legal transmission limitations, the use of Anti-Jam algorithms in a custom front-end architecture providing protection to a GNSS and INS navigation sensor is simulated via hardware in the loop (HWIL) to mimic hostile navigation environments. The HWIL system consists of multiple calibrated software-defined radios (SDRS), propogation delay systems, GNSS/INS systems, timing, network, and processing devices. Each controlled by custom or open-source software to create a system capable of simulating transmitted signals as would be seen in a wavefront scenario. This system demonstrates moderately realistic signal source localization. This conceptual platform, designed to observe and localize a signal, requires several sensors for observing its own location in the challenged RF environment. The suite of sensors on this platform would include a GNSS and INS system to provide both position and attitude that utilizes a fixed array of antennas. The array, known as a controlled reception pattern array(CRPA), is designed for the navigation band of choice as well as the signal of interest. The CRPA, utilizing mulitple signal classification (MUSIC), provides a direction of arrival (DOA) to the transmitting source. The combination of the platform position, attitude and DOA collectively provide the required information to generate estimates of the transmitter location. The estimation methods referenced and derived include batched and continuous estimation techniques utilizing the combination of the available observables on the theorized platform. The use of closed form solutions with the noisy measurements are used only as initialization points for the batch and continuous estimators. The estimation is done in two and three dimensions for various esimators. These methods are selectivly compared based on the applied estimation technique. The comparisons are divided into two groups, stochastic and instantaneous. The instantaneous group is used as a method of initialization of the stochastic filters but should also

be considered as an estimate method in multiple observer cases. The centroid algorithm provides moderately better results than other methods reviewed in the simulation. The stochastic solutions are compared in the second group. The maximum liklihood estimator provides the best solution consistently. While the particle filter method and extended kalman filter provide similar results, they fall victim to different failure modes induced by the observer path.

Acknowledgments

I would like to thank my family and friends that supported me through the late nights and time sacrificed. Thank you for your patience as I spent my time focusing on work and writing.

To my parents, Thank you for being patient with me. The research and work became a large part of my daily life which you had to hear the difficulties of and not as many of the successes. Most of which were achieved in the early hours of the morning.

To my friends who were right along side me, Tanner, Scott, Josh, Sam and Drew. Thank you for helping me along the way with various problems and frustrations. Thank you for also helping to maintain much needed work-life balance.

I would like to thank my professors, Dr. Scott Martin and Dr. David Bevly, for both the opportunity and patience working with me. I have learned as much, if not more, during my masters as I did during my undergraduate degree.

Everyone played very significant roles in both supporting me as well as helping me complete the research and writing.

Contents

List of Figures

List of Tables

Chapter 1 Introduction

Navigation requirements in the modern world are constantly evolving. Modern navigation solutions typically consist of a global positioning system, a system capable of providing a location relative to the earth. These global navigation solutions are often provided by orbiting satellites transmitting radio signals. The positioning systems suffer from weak signals due to the range between transmitter and receiver. The weak signals are commonly subject to interference sources. Other navigation methods can be used in conjunction to aide these systems. This is a common practice in the navigation field. Although these other solutions exist, they tend to suffer from different types of errors that satellite navigation systems do not suffer from. The use of these systems provide solutions for extended time periods. Low power systems Signals emitted from existing systems can be used to aid navigation systems by introducing further ranging information or bearing information. These secondary navigation signals come in many forms. Cellular signals and WIFI signals are both examples of these secondary signals. In order to use these signals as way points in the aided navigation, the observing signal must know where the signal is coming from. The signal source location may be transmitted in the signal for cooperative communication but not all signals are conducive to communication. These other signals are typically directed at a particular user and causes some form of interference for the navigation equipment. These sources of interference can be localized from an observer. The methods collected here combine several type of algorithms to localize and estimate a signals source from a single observing platform.

1.1. Background and Motivation

Modern technology is relied on in nearly every industry. In the industries that require mobility, navigation equipment is a common component of the utilized technology. Some form of navigation is required in all mobile applications in both the civilian and military environments.

In many cases, satellite navigation is sufficient for the application. These global navigation satellite systems (GNSS) define several ubiquitous systems. Each GNSS system utilizes satellites transmitting a dedicated navigation signal for receiving equipment to decode and estimate its own position. Six GNSS systems exist in operation today. The United States, Russia, China, European Union, India and Japan each have unique systems[14]. Table 1.1 shows a simple summary of the systems from each country. These systems have similar methods of operation but vary by signal frequency, band, coverage and availability.

Table 1.1: Current GNSS systems

System	**BeiDou**	**Galileo**	**GLONASS**	**GPS**	**NavIC**	**QZSS**
Country	China	European Union	Russia	United States	India	Japan
Satellites	35	22[1]	28	32	7	7
Coverage	Global	Global	Global	Global	Regional	Regional
Center Frequency (MHz)	1561 1580	1164 1260	1602 1246	1575 1227	1164 2483	15754 12276
Precision (Public)	10m	1m	7.4m	5m	5m	1.5m

While each of these systems have different frequencies and operational bands, they have somewhat similar positioning results during basic operation. There are several other types of satellites that are also used but not listed here such as SBAS, which is used as augmenting signal from deeper in space. This satellite aids in a similar was as QZSS aids GPS's constellation.

Each of these constellations use different signals and encoding, resulting in different hardware requirements for each constellation. Dedicated navigation devices, such as Ublox receivers, are capable of tracking signals from each of these systems while using an antenna covering the required bands.

While there are numerous satellites in operation, they are not always satisfactory for a given scenario. In scenarios where the GNSS devices are insufficient, the receivers can be aided by other navigation signals and sensors. Aiding GNSS devices can come from other signals, sensors or other GNSS receivers. This navigational aid is particularly useful when the GNSS signals produces poor or insufficient results. In many cases, an inertial measurement unit (IMU) is used. This is one of the more common forms of navigational sensor aiding. The use of other signals is very common as well. External signals include other constellations, dedicated short-range communications or radar. Each of these signals when combined with a GNSS receiver provides information that the GNSS receiver cannot. These are only two of many ways that a GNSS receiver can be aided. Many researched areas include most permutations of GNSS, IMU/Gyro, Camera, Radar, LiDAR and DSRC. Many efforts exists to reduce complexity of combining these sensors but are often still computationally heavy when power or time limitations are a concern. Radio systems that communicate in both directions can provide further information than that of just GNSS. By sharing power received measurements with the transmitting device, devices can utilize spatial processing to resolve direction relative to each device. This is seen in many modern day wireless routers under the 802.11.n specification. This is known as beam-forming. This directional information can be used to find relative locations of devices on the network. Direction to uncooperative signals can also be found using a modified version of these techniques. Methods to find the direction to a signal require multiple antennas receiving the signal of interest. Combining these types of signal processing algorithms, along with aided GNSS sensors, estimations can be made passively.

Sensor aiding is commonly seen in conjunction with Bayesian filters. These types of filters use state models and sensor measurements with stochastic probabilities to produce a more accurate result [41][25]. These filters have various forms that excel in different scenarios. As the stochastic assumptions change, the filters are adapted to different scenarios. One form of the filter is the extended kalman filter (EKF). The EKF is focused for nonlinear state models and nonlinear measurement models using a Gaussian distribution probability. EKFs utilize linearization techniques to produce better results with the nonlinear models within certain operational ranges. The system model relates the states of the system to inputs while the

measurement model relates the sensor measurements to the states. These models are application dependent and vary from system to system. The models are mathematically derived from theory of operation, known kinematics, or assumptions. Error quantification for a model is often difficult to derive and can often be found empirically.

As autonomous devices become the standard in any industry, the use of sensor aided navigation will only become more useful. Industries operate in vastly different environments. These environments require sensors that excel in the different locations. An example of additional navigational aids are in the forestry industry. One of these challenging navigational environments is beneath the forest canopy. This does not necessarily make GNSS systems useless but does severely degrade the performance. The Global Positioning System (GPS) error is typically below three meters with adequate satellite coverage[35]. The error in canopy coverage can commonly grow up to an additional eight meters [21]. This makes accurate position solutions difficult to achieve. In order to continue toward completely autonomous systems, these navigation systems must be aided. Navigation dependent autonomous systems are being envisioned by leading forest industries[33].

To show motivation by example,Consider a system of devices where the primary device will find the gloabl position of secondary devices and the tertiary devices are in communication with several secondary devices. The primary system can operate above the forest canopy where GNSS signals are significantly stronger. The secondary devices can operate as below canopy base stations assumed to be incapable of finding its own position with GNSS signals. The tertiary system, as depicted from[33], can be any other device requiring moderately accurate position operating below the canopy. Figure 1.1 shows an example of this scenario.

Figure 1.1: Primary, secondary and tertiary systems

In this example, the primary system is a drone capable of solving its own position and attitude via aided GNSS. The secondary system is a temporary transmitting station and the tertiary system is a navigation dependent piece of equipment capable of communications with the secondary systems. The tertiary system is the autonomous device similar to the system under development by australian forestry companies[33].

The primary system can pass the global location of the secondary system to each of the secondary system devices. The primary system would localize each secondary device once since they are static. The secondary system, remaining stationary, is capable of providing below canopy navigation for the tertiary systems.

To further motivate the purpose of localizing a signal, airports are commonly victims of signal interference, both intentional and unintentional. Airports utilize a ground based augmentation system (GBAS) to aid landing planes with radio signals. As passenger and cargo jets travel in and out of many airports everyday, they are vulnerable to these signal interference sources. While many different airliners have many different sensors, degradation of one of the sensors puts many lives at risk.

These devices are commonly found on the internet and can even sometimes be bought locally on the order of hundreds of dollars. Figure 1.2 shows an example of several widely available devices.

Figure 1.2: Common jamming devices that are used in vehicles

These are referred to as a personal privacy devices (PPD) . Many PPD users are motivated due to being tracked for various reasons. Commerical vehicles are commonly tracked using GPS to ensure safe driving. PPD users can utitlize these devices to stop tracking efforts. The 10mW device is capable of a range up to 400m[16]. Each additional PPD user can cause issues for GNSS devices on airliners due to radio signal propagation behaving differently on the ground. Due to this behavior ranges are typically further vertically than horizontally given an isotropic radiation and due to signal occlusion. Heavily populated airports are more likely to have these devices in the nearby vicinity.

While PPDs may seem to be small weak devices, the Federal Aviation Administration (FAA) and the Federal Communications Commision (FCC) worked together for years in order to locate a PPD used by a commercial trucker. The trucker frequently drove past the airport with a PPD installed. The device would commonly cause issues with the GBAS. It took nearly two years for the interference source to be found[18]. These systems can cause GNSS receivers to be unable to estimate a position or even make them more vulnerable to other attacks.

Outside of civilian industries, the military could also benefit from the localization of a signal through the combination of a navigation system utilizing a system capable of finding the direction to a device to locate the signal source.

1.2. Prior Art

Current technologies to locate a signal range from military systems to every day home devices such as a wireless router. Military systems utilize radar or situational awareness systems to find and track signal sources. These systems can use trilateration, triangulation or both. Trilateration uses estimated ranges from multiple receivers which is similar to current navigation systems. Triangulation uses multiple observation points with relative direction information to produce a location. These methods are also commonly used in systems with multiple observers. There number of systems utilizing a

British Aerospace systems (BAE) produced a system capable of localizing an electronic emitter. This system was first tested in 2015[38]. This is one of several signal intelleigent systems used by multiple countires. The information available on this system is limited due to its application.

This type of localization analysis is commonly found in radar systems. The earliest radar publications related to this topic are from the mid 19th century. These methods incorporated both range and bearing. While many radar systems have a range component to it due to the known nature of the signal, the methods of estimation are still appilicable to this proposed platform when the range is not used. Systems described in [22], [32] and [] utilize non-range based estimation techniques. The latest bearing only solutions provide a new type of localization without maneuvering[22].

Other systems capable of localizing a system include most home networks. Wi-Fi positioning system (WPS) uses local WiFi networks to aid in a devices current position. This type of system requires a cooperative signal and uses both directional and range information for the receiver device. The access points utilize beam-forming over a search space to find the direction the user receives the highest power. This reveals the relative direction to the access point from the device[36]. A range can be found with the transmit power, receive power and a signal propagation model [37]. This information is available to a cooperative signal. This is referenced as the received signal strength indicator (RSSI) . Figure 1.3 shows an example of this type of networked system.

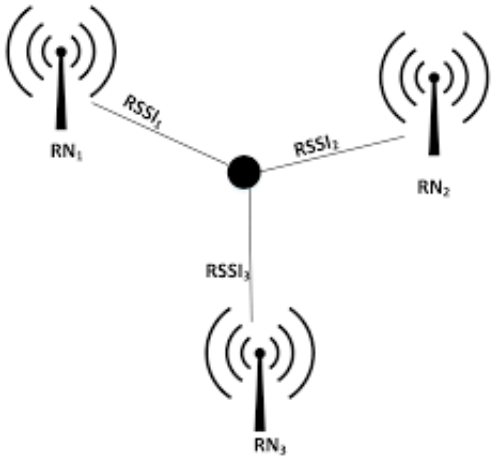

Figure 1.3: Received Signal Strength Indicator represented in a physcical network

The combination of this information allows a device to produce a local position relative to multiple cooperative wireless networks access points.

1.3. Contribution

This thesis provides an analysis of the use of a single observing platform to localize signal sources and the related algorithms. It also provides a prototyped hardware simulation system that is capable of emulating the scenario considered using relatively low cost systems. The platform's relevant navigation results and directional components are analyzed with respect to the potential solution proposed for the observing platform. This conceptual device utilizes an estimation filter to produce localization of a transmitting signal of interest. Relevant device parameters are explored to inspect the resulting localization solution produced by the chosen sensor system and parameters. As problems are explored, solutions and algorithms are utilized to create a collection of subsystems to produce a final result, the source location. Based on the prior art, most formulations of the problem do not consider the design aspects of the observation platform as part of the localization simulation. Prior art related to the navigation methods or MUISC is well documented. The localization methods are documented in but cover a wide range of observer platforms typically consisting of multiple observers. This thesis looks into the design of the platform and how a few of the key platform design parameters impact the DOA and how a specifc design is capable of localizing a signal using several algorithms.

1.4. Outline

The first chapter has introduced the concept of finding a signal in an environment that has degraded or low quality GNSS signals and motivates the importance of navigation in a challenging environment. This chapter also covers some of the current research in related topics. This research also outlines several other related industries that utilize similar methods. Chapter two covers the basic concepts of GNSS, specifically GPS and its use case for this thesis. Chapter Three discusses the use of GPS to find the pose, position velocity and attitude, of the primary device via multi-antenna arrays. Chapter four shows the basics of finding the direction a signal is coming from via estimation. Chapter five discusses estimation of the the signal source location using information available only at the primary device as shown in previous chapters. Chapter six discusses a simulation and the results of the simulation while chapter seven discusses the implementation, test environment and results for a real time system. Chapter eight concludes the thesis and covers work that may be of future interest. The appendix contains further information on various topics related to the thesis and other work attempted.

Chapter 2 Global Positioning System

Global Positioning System (GPS) is the United States' GNSS system. This system was originally launched in the 1970's over a series of orbital satellite launches. These launches started in the 70's and has extended to as recently as 2018[42]. As the lifespan of satellites have been reached, new satellites have been launched. The satellites, commonly referenced as the space component of the GNSS system, are distributed in six different orbits approximately 22,000 Km from earth[42]. The next component consists of the control system for GPS. This system monitors and corrects errors in the satellites from Earth. The final segment is the receiver, which is for the end user. The original intention for GPS was military applications. It was later opened to the public under the Reagan administration. The system was originally limited by selective availability. This reduced the public accuracy of the system. The ending of selective availability in 2000 began an era of commercial products that could better utilize GPS signals. As receivers became more affordable, they were implemented into many different devices such as cell phones, cars, drones and watches. A large majority of electronic products today have GNSS receivers in them and are capable of providing the user with a global position within a few meters of the true position [30]. While these systems are highly utilized, it emphasizes the reliance on the system across many industries. GNSS systems are a one directional communication system that allows the receiving device to decode information and can estimate its position any where on the earth. This is known as positioning and is fundamentally similar to localization which is discussed later. Positioning benefits from creating a global solution rather than a local solution. While local solutions are useful when referencing relative positions, the global solution allows for repeatable positions over extended periods of time.

2.1. GPS Signals

GPS signals are transmitted from the satellites in orbit at two main frequencies. While several other signals exist, this thesis focuses on the primary civilian signal, L1. The frequencies have a fundamental component created by the atomic clocks aboard the satellites[30]. Equations 2.1, 2.2 and 2.3 show the relationship between the common component, f_o, and broadcast frequencies, L_1 and L_2.

$$f_o = 10.23MHz \tag{2.1}$$

$$f_{L1} = 154 * f_o = 1575.42MHz \tag{2.2}$$

$$f_{L2} = 120 * f_o = 1227.60MHz \tag{2.3}$$

Each signal consists of three parts. First, the carrier signal which is a sine wave at the broadcast frequencies. Second is the navigation data. The navigation data is at a rate of 50 Hz. This data contains information regarding the satellites, clocks, and Ephemerides. This data structure is defined by the IS-200, a published document defining the interface specifications of GPS[17]. The third section is the spreading sequence. The spreading sequence is what makes each satellite signal unique. The spreading sequence, also known as the Gold codes or psuedo-random sequence (PRN), are deterministic sequences with noise like qualities[1]. These prn codes are transmitted at 1.023 MHz (for the L1 signal)[44]. Figure 2.1 shows what the resulting time domain signal appears as.

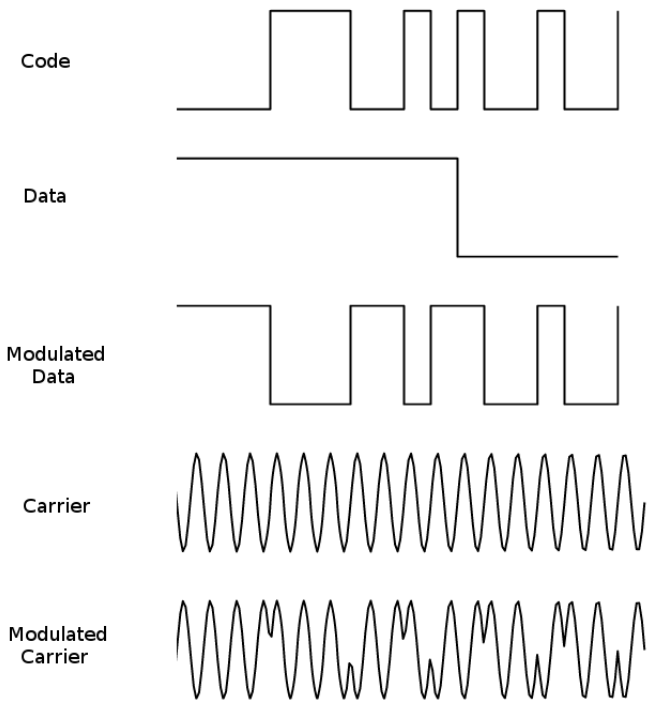

Figure 2.1: GPS Signal in the time domain

The first signal C/A Code, the second is the navigation data. The third signal shown is the modulated combination of the previous two signals. The carrier is shown as well below the C/A and navigation modulated signal. This signal is then modulated with the carrier frequency to produce the final signal shown. This is the GPS signal that is received at the antenna for each satellite and antenna combination.

Acquisition and tracking of GPS signals is a heavily documented and researched topic, the process is done by all GPS receivers. While the process could be discussed in detail, the scope of the thesis is focused on the estimation of the signal sources and combining the information at the observer. The reader is directed to [44],[29],[8],[45] for acquisition and tracking information related to scalar, vector, SDRs and clock related acquisition and tracking information respectively.

2.2. Receiver Architecture

Having discussed the basic structure of the signal, it is important to layout the digitization of the signal at the observer. While this is arguably out of scope, the topic is extremely important at the estimation of the attitude, bearing and signal source position. The GPS signals are very weak signals being received at approximately -158 dBm[44]. While this is an extremely weak signal, several methods are commonly used to mitigate signal power issues. These GPS radio signals require several pieces of equipment that allow the Radio Frequency (RF) signal to be converted to a final position. The use of additional hardware reduces signal power based issues. In a basic receiver architecture, the signal starts at the receive antenna and passed into an amplifier. Following the amplifier, the signal is filtered then passed into a down converter. This shifts the frequency of the signal to an intermediate frequency (IF). This intermediate frequency is filtered again and digitized at an ADC. The signal is then passed into the processor for acquisition and tracking. The receiver acquires and tracks each individual satellite signal from the filtered IF data. Multiple methods of acquisition and tracking exist but are not discussed at length due to the comprehensive nature of the topic as mentioned previously (refer to [44],[29]). Figure 2.2 shows an example of a basic receiver architecture.

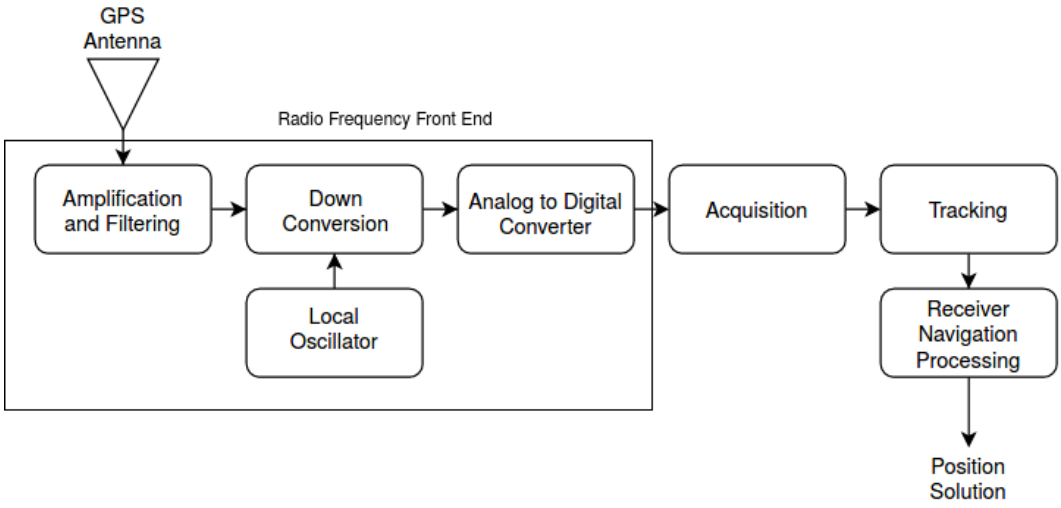

Figure 2.2: Basic GNSS receiver architecture

This can be separated into different subsections. The RF front end includes the amplification and filtering through the analog digital converter. The acquisition and tracking loops are the heart of the GNSS receiver and each have their own subsection. The receiver navigation processing is a subsection as well due to the many different methods that can be used here.

2.3. RF Front Ends

RF Front Ends are used in many applications, not just in GNSS receivers. The purpose of a front end is to prepare the signal to be used for its purpose in the device. In the case of many GNSS receivers, it is to receive satellite signals amplify and filter, then frequency shift before amplification and filtering again. Addressing signal power is typically the first concern of the front end. GPS is a weak signal transmitted from orbit. According to the GPS techincal specifications, the signal is ensured to be above -158.5 dBW. This is far below the thermal noise floor of many electronic systems as defined in Equation 2.4[20].

$$\eta_{Floor} = 10 * log_{10}(k * t_0 * 1000) + \eta_{Rec} + 10 * log_{10}(BW_{Rec}) \tag{2.4}$$

In the equation, k is Boltzman's constant. T_0 is the antenna temperature. η_{Rec} is the noise floor of the receiver and the receiver bandwidth is BW_{Rec}. Bandwidth limitations in relation to the noise floor are a concern due to the spread spectrum of the gps signal as seen in 2.3

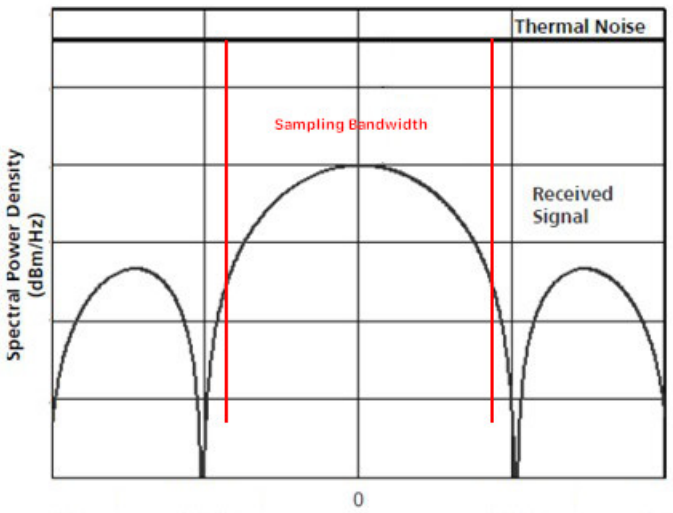

Figure 2.3: RF chain for a front end system

Generally, higher sampling bandwidth results in a higher noise floor. Ideally the narrowest bandwifth acceptable for the signal of interest should be used while also minimizing IF signal impact. Figure 2.4 shows the break down of a front end in greater detail than the GNSS receiver architecture.

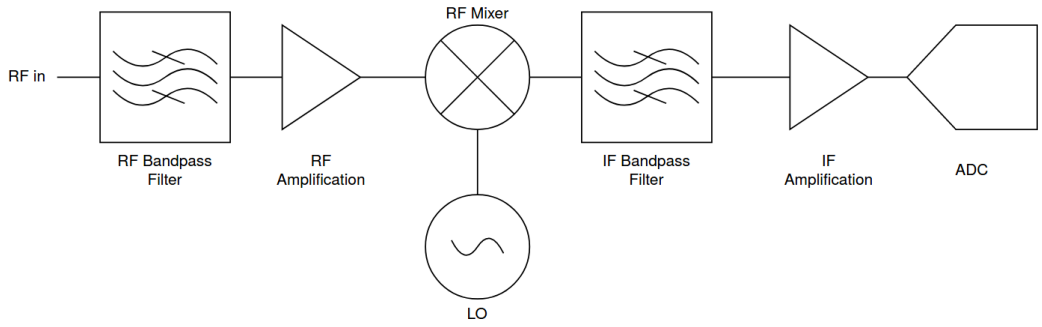

Figure 2.4: RF chain for a front end system

Following the antenna, there is filtering and amplification at RF. A low noise amplifier (LNA) is typically used as the amplification device. Low noise levels are vital to allow the signal to be able to be used efficiently. Amplifying the signal allows the system to be able to receive the signal when the system's analog to digital converter (ADC) is incapable of quantizing on the original signal.

Front ends also commonly convert the signal to a different frequency. This is known as a superheterodyne front end[3]. Down conversion allows the ADC to be able to capture the signal at a much lower frequency. In GNSS receivers, the goal is to reduce the frequency the ADC needs to capture. Figure 2.5 shows the RF chain of a typical front end device.

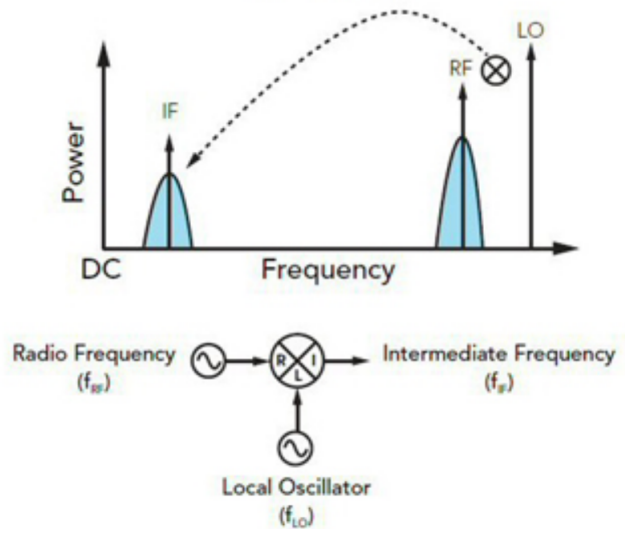

Figure 2.5: Frequency Represnentation of Down Conversion

The local oscillator (LO) and the original RF signal are mixed to produce the IF signal. Filtering is used to remove images from the signals as well as reduce requirements on the amplification devices [3]. Figure 2.5[15], shows the resulting frequency domain of the RF chain. When the LO is a higher frequency than the RF signal, the signal frequency is shifted down as shown in figure 2.5.

Equation 2.5 represents the original RF signal.

$$s(t) = A_{RF} * (sin(2 * \pi * f_{RF}) + cos(2 * \pi * f_{RF})) \tag{2.5}$$

Both the RF signal and LO signal can be represented by Equation 2.5 with the associated amplitude and frequency. After frequency shifting, the signal is moved to a new frequency along with a signal image in the frequency domain. This relationship can be shown in Equation 2.6.

$$s_{IF}(t) = A_{RF} * A_{LO} * (sin(2 * \pi * (f_{RF} + f_{LO})) + cos(2 * \pi * (f_{RF} - f_{LO}))) \tag{2.6}$$

The mixed result of the signals produces frequency components that are not desired in the final signal. Secondary filtering at the intermediate frequency is used to mitigate these

undesired components of the signal. The relationship between the IF and signal frequency is seen in Equation 2.7

$$f_{LO} - f_{RF} = f_{IF} \tag{2.7}$$

These down converted and amplified signals should be within the ADC's capable range. The signal is passed through band pass filtering before the ADC digitizes the signal. Figure 2.4 shows these filtering systems. The samples are then passed onto the next portion of the receiver to begin acquisition, tracking and positioning. Further reading on acquisition and tracking can be found in many different sources. [44],[29],[40],[9].

2.4. Receiver Pose

As previously discussed, the GNSS system produces a global position for a given antenna using signals generated from multiple satellites. After the signal has been decoded, the information from this signal is used to find the antenna position. This does not provide any information for the orientation of the antenna. In order to produce information about the orientation, multiple GNSS antennas must be used. Antennas placed on the body of a platform can produce the necessary attitude information. The combination of the position and attitude is referred to as pose. Attitude represents the three dimensional orientation of an object in space. The three dimensions are typically represented by yaw, pitch and roll, collectively labeled euler angles. The combination of these angles in rotation matrices can be used to rotate the body coordinate frame to a global coordinate frame or a chosen navigation frame. This rotation can be used to rotate information from one frame to the next. The euler angle definition fails in some cases due to gimbal lock. Gimbal lock is discussed in the appendix and other noted sources [5].

2.4.1. Pseudorange Positioning

Positioning a receiver to a three dimensional location requires at least three satellite receivers when using a perfect clock. Figure 2.6 shows this scenario.

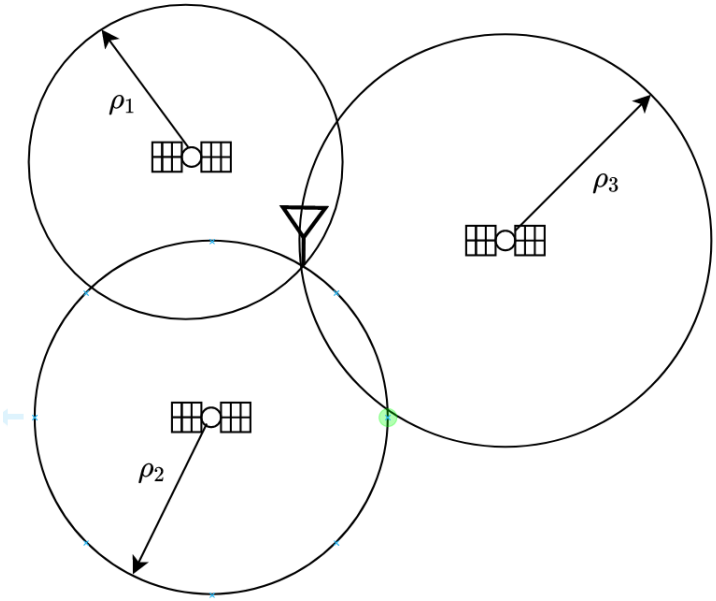

Figure 2.6: Range Positioning with three satellites

The centers of each circle represent the location of the satellites. The intersection of the circles represents the location of the antenna receiving the signals. The radius of the circles are proportional to the range from the satellite to the user. The receiver estimates the range to each satellite, ρ_n.

The satellite positions are known to the user through the decoded information on the satellite signal. With the known locations and ranges of each satellite, a position of the receiving antenna can be estimated through iterations of least squares (ILS). Receiver hardware introduces an unknown clock bias. This clock bias can be estimated but requires an additional satellite.

The range to a given satellite is found with a transmit time, t_{st}, which is given in each satellite's signal. The receiver is using its own time, kept by a local clock, to approximate the time between signal transmission and reception. Equation 2.8 shows this relationship.

$$\rho_{i,true} = C * (t_{receiver} - t_{i,st}) \tag{2.8}$$

This elapsed time is multiplied by the speed of light to represent the true range to each satellite.

The subscript st represents the time at a given satellite. The subscript i denotes a specific satellite. In practice, the true values are not available and are also biased. The measured values are related to the true values as shown in Equations 2.9 and 2.10.

$$t'_{i,st} = t_{st,i} + b_i \tag{2.9}$$

$$t'_{receiver} = t_{receiver} + b_{receiver} \tag{2.10}$$

These equations show an additional bias in both the satellite clock and the receiver clock measurements. The satellite clock bias has corrections provided from the U.S. government through the signal. The receiver clock bias is the value that must also be estimated with the position. The measured pseudorange is defined in Equation 2.11.

$$\tilde{\rho}_i = \rho_{i,true} + c * b_i + c * b_{receiver} + c * T_i + I_i + M_{receiver} + v_{receiver} \tag{2.11}$$

The measured value has error introduced from clock bias errors, atmospheric errors (T_i and I_i), receiver noise (v_i) and multipath errors ($M_{receiver}$). Satellite positional error has little impact on the measurement and can fall within the receiver noise. The clock error for the satellite is corrected in the data transmitted. The receiver clock bias must be estimated in the positioning solution. The atmospheric errors can be accounted for in some systems such as dual frequency systems but this is not required[24]. Finally, the receiver psuedorange noise is a function of the bandwidth, carrier to noise ratio and integration period as shown in sources [29],[44]. The pseudorange measurement model relates the position estimates in Earth Centered Earth Fixed (ECEF) coordinates to the range measurements from each satellite. This is seen in Equation 2.12.

$$\hat{\rho}_i = \sqrt{((x_i - \hat{x}_{rcvr})^2 + (y_i - \hat{y}_{rcvr})^2 + (z_i - \hat{z}_{rcvr})^2)} + b_{rcvr} \tag{2.12}$$

The bias term at the end of the equation is the clock bias of the receiving device. This term is common among each of the range equations. Differentiating Equation 2.12 produces Equation 2.13.

$$\delta\rho_i = \frac{(x_i - \hat{x}_{rcvr}) * \delta X_{rcvr} + (y_i - \hat{y}_{rcvr}) * \delta Y_{rcvr} + (z_i - \hat{z}_{rcvr}) * \delta Z_{rcvr}}{\sqrt{((x_i - \hat{x}_{rcvr})^2 + (y_i - \hat{y}_{rcvr})^2 + (z_i - \hat{z}_{rcvr})^2)}} + \delta b_{rcvr} \tag{2.13}$$

This iterative form represents the relationship for a single satellite. Combining the equation into vector form, produces Equation 2.14 where Equation 2.15 simplifies the vector form.

$$\delta\rho_i = \begin{bmatrix} \frac{x_1 - \hat{x}_{rcvr}}{\hat{r_1}} & \frac{y_1 - \hat{y}_{rcvr}}{\hat{r_1}} & \frac{z_1 - \hat{z}_{rcvr}}{\hat{r_1}} & 1 \\ \frac{x_2 - \hat{x}_{rcvr}}{\hat{r_2}} & \frac{y_2 - \hat{y}_{rcvr}}{\hat{r_2}} & \frac{z_2 - \hat{z}_{rcvr}}{\hat{r_2}} & 1 \\ \vdots & \vdots & \vdots & \vdots \\ \frac{x_i - \hat{x}_{rcvr}}{\hat{r_n}} & \frac{y_i - \hat{y}_{rcvr}}{\hat{r_n}} & \frac{z_i - \hat{z}_{rcvr}}{\hat{r_n}} & 1 \end{bmatrix} * \begin{bmatrix} \delta X_{receiver} \\ \delta Y_{rcvr} \\ \delta Z_{rcvr} \\ \delta b_{rcvr} \end{bmatrix} \tag{2.14}$$

$$\hat{r_i} = \sqrt{(x_i - \hat{x}_{rcvr})^2 + (y_i - \hat{y}_{rcvr})^2 + (z_i - \hat{z}_{rcvr})^2} \tag{2.15}$$

This is the iterative model that is used in the least squares process relating the measurements to the states. Using this relationship, the iterative least squares can be repeated using Equation 2.16 until the change in states are small. After each iteration, the values are updated and repeated.

$$\delta\bar{X} = (H * H^T)^{-1} * H^T * \delta\rho_i \tag{2.16}$$

The matrix H represents the observation matrix. This contains the relative directions of the satellites to the receiver. This matrix is commonly used to find the dilution of precision (DOP) as defined in Equation 2.17.

$$DOP = (H * H^T)^{-1} \tag{2.17}$$

The DOP is a measure of the accuracy of the estimated position state. The DOP is more useful in a navigation frame such as ENU or NED. The diagonal of the resulting matrix represents the potential error that could exist in that state as shown in equations 2.18 to 2.20.

$$\sigma_x^2 = DOP_{1,1} \tag{2.18}$$

$$\sigma_y^2 = DOP_{2,2} \tag{2.19}$$

$$\sigma_z^2 = DOP_{3,3} \tag{2.20}$$

Typically, the error of the position is around three meters given an adequate DOP [44]. This error range is important when creating pose information as shown later in this chapter.

2.4.2. Carrier Phase Positioning

Carrier phase positioning uses the carrier signal of GPS. The base frequency component of the signal is a sine wave as shown previously in figure 2.1. The information available here is limited due to the repeating nature of a sine wave. In order to position with the carrier phase signal, the phase must be measured by a phase lock loop.These methods such as Precise Point Positioning or differential positioning can be used to position on the order of one tenth of the carrier wavelength [13]. After acquisition, receivers use tracking to be able to continuously receive data from the signal. These tracking loops compare the received signal to a replicated signal to measure a phase error. This phase error allows the receiver to know approximately where in the cycle the signal is. This information is still not enough to be able to position. The total number of cycles is still required. This value can be reduced using the LAMBDA method[43]. The combination of the total cycles and the phase produce a range to each satellite. Equation 2.21 shows the representative components of the measurement while Equation 2.22 shows the carrier phase estimation model.

$$\phi = \rho_a^s + c * dt_a^s + c * dt^s + T_a^s - I_a^s + \lambda * N_a^s + M_{a_\phi}^s + v_{a_\phi}^s \tag{2.21}$$

$$\Phi = \lambda * (N_i + \phi_i) + \eta_i \tag{2.22}$$

These equations result in meters to each satellite.

The measurement model consists of the true range, ρ_a^s, the receiver clock bias and satellite clock bias scaled by the speed of light, dt_a^s and dt^s respectively. T_a^s and I_a^s represent the troposphere and ionospheric components respectively. The multipath is represented by $M_{a_\phi}^s$. The last term, $v_{a_\phi}^s$ represents the noise of the measurement. Each term with a superscript or subscript reference each individual satellite or antenna respectively.

Here, λ represents the carrier wavelength, N represents the whole cycles to a satellite and ϕ_i represents the fractional cycle for a satellite signal. The associated noise on a carrier measurement is a function of the tracking loops within the receiver and is represented by η_i. The tracking loops are a heavily researched topic in [44],[29] and [35]. Equation 2.23 shows the relationship between several receiver parameters and the resulting fractional phase noise of a signal[35][7].

$$\sigma_{PLL} = \sigma_{noise,interference}^2 + \sigma_{phasenoise}^2 + \triangle\theta^2 \tag{2.23}$$

where $\sigma_{phasenoise}$ is the noise associated with the receiver clock hardware and $\triangle\theta$ represents the change in phase during a loop update along the direction of the line of sight to a satellite [6]. $\sigma_{noise,interference}$ is represented in Equation 2.24 where B_l is loop bandwidth, CN_0 is the carrier to noise ratio and γ is the fraction of total signal power in the component being tracked.

$$\sigma_{noise,interference}^2 \cong \frac{B_l}{\gamma * CN_0} \tag{2.24}$$

These associated errors are assumed to be Gaussian and are not biased. The clock bias terms can be mitigated with methods such as differencing, known as differential GPS (DGPS) . Using the differencing method across multiple antennas, Equation 2.21 can be reduced to **??**.

$$\triangle\phi_{12} = \rho^s_{12} + c * dt_{12} + \lambda * N^s_{12} + v^s_{12} \tag{2.25}$$

This model combines the atmospheric noises with the measurement noise and ignores the multipath component. Multipath can be mitigated using different techniques across multiple antennas [27].

This equation has an unkown number of cycles represented by the true distance between the antenna and the satellites. This value is represented in the equation by $\lambda * N$. In this case, the number of full cycles is constrained to an integer value.

Limiting the distance between the two antennas to less than a wavelength can reduce this equation further to drop the integer wavelength to zero. Equation 2.26 shows this result.

$$\triangle\phi_{12} = \rho^s_{12} + c * dt_{12} + v^s_{12} \tag{2.26}$$

This wavelength limitation is shown to be relevant when considering the AOA as shown in a later chapter.

Chapter 3 Platform Attitude Determination

Attitude is the description of the physical orientation of a body in three dimensional space. Fusing measurements in the three dimensional systems require information to be in common coordinate frames. Information produced at the body frame must be rotated into the desired navigation frame using the attitude information. In order to do this, the relative body frame attitude must be found. This can be done with two unique nonparallel vectors attached to the body in question. These vectors are then compared to another reference frame such as North East Down (NED) or East North Up (ENU). Attitude determination using only GNSS measurements requires at least three antennas in independent directions to produce the rotation at a single instant.

Use of multiple signal paths require each antenna to have its own signal processing to produce the positions and resulting vectors. This can be done by a single device that utilizes a single oscillator. This reduces ambiguities in the measurements from antenna to antenna by removing additional clock biases. This is sufficient for the pseudorange attitude solution approach. The carrier phase measurement system requires the integer estimation in order to produce the body vector beyond half a wavelength [7]. Simplifying the ranges of operation for each method, the psueduorange method is the simplest but requires a large antenna separation. The carrier phase method requires more processing and fairly accurate initial conditions but can be reduced to much less than a wavelength.

The pseudorange system is commonly seen on larger systems that require attitude such as aircraft carriers. This system is called JDAP and is used in transmitting an accurate attitude of the carrier to the landing aircraft. In shorter antenna separations,

Defining the attitude of a body using only GPS measurements requires a three planar antenna system in two of the principle directions. One antenna is chosen as the base antenna.

The two remaining antennas are auxiliary antennas. Differencing the position of the two auxiliary antennas with the main antenna produces the required vectors to represent the euler angles. These differential vectors are used to produce the required attitude for the the body frame which can be rotated to a different frame. Figure 3.1 shows an example of an antenna configuration capable of producing all three euler angles independently.

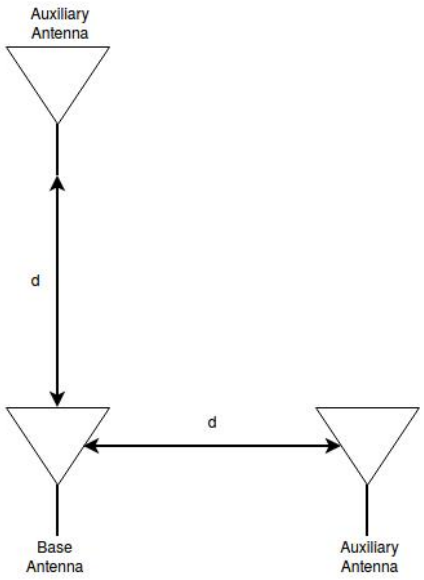

Figure 3.1: Antenna Configuration

The antennas shown are inline with the principle axes of the body in question. Equation 3.1 shows the difference of the main antenna position and auxiliary antenna two in the three dimensional vector form.

$$\begin{bmatrix} \triangle X_{NM} \\ \triangle Y_{NM} \\ \triangle Z_{NM} \end{bmatrix} = \begin{bmatrix} X_N \\ Y_N \\ Z_N \end{bmatrix} - \begin{bmatrix} X_M \\ Y_M \\ Z_M \end{bmatrix} \tag{3.1}$$

The subscript of $\triangle X_{NM}$ represents the position difference between antenna N and the main antenna M in the x direction. The same notation follows for the y and z directions in the body frame. For the research presented, the antenna vectors coincide with the positive x and positive y axes of the body frame.

Generating these two vectors allow the body attitude to be defined completely with instantaneous measurements. This information must be translated into different coordinate frames to relate to other systems in a global frame. This can be done with rotation matrices or quaternions.

3.1. Coordinate Frame Rotations

Different applications can benefit from different coordinate frames. A device that is constrained to a building does not need global coordinate frame solutions where as a plane or car would benefit from a global solution. There are several commonly used frames in navigation including NED, ENU, and ECEF. These frames are chosen within different fields as a standard. ENU and NED are both frames defined from a single point while ECEF is defined with respect to the Earth. Many other frames exist but are not within the scope of this thesis. Converting between a local or navigation frame to a global frame can be done with direction cosine matrices (DCM). A DCM utilizes mathematical manipulations to transform across coordinate frames using the attitude representation between coordinate frames. DCMs have a limitation termed gimbal lock.

In the three dimensional case, the DCM is the product of three different rotations about the principle axes of the original frame as shown in Equation 3.2.

$$\begin{bmatrix} X_{NAV} \\ Y_{NAV} \\ Z_{NAV} \end{bmatrix} = \begin{bmatrix} R_{BodytoNAV} \end{bmatrix} \begin{bmatrix} X_{Body} \\ Y_{Body} \\ Z_{Body} \end{bmatrix} \tag{3.2}$$

Each rotation is with respect to a specific axis in the body frame and its intermediate frames. Figure 3.2 shows the rotations with respect to the body frame coordinate system.

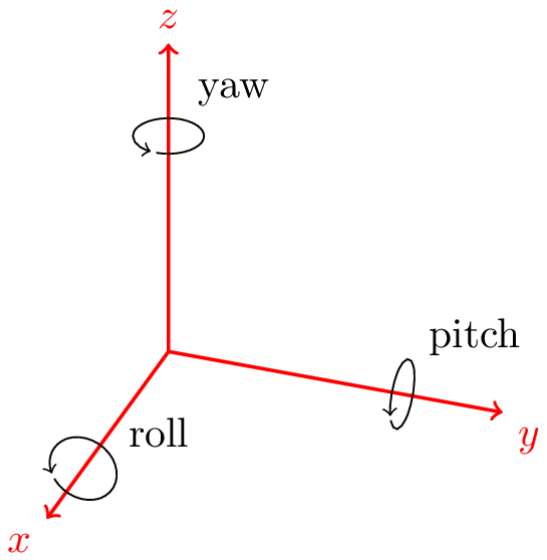

Figure 3.2: Euler angle rotations on a coordinate frame

Considering the figure, the z axis must point out of the top of the body, the y axis points out the side of the body and the x axis points out the front. The euler angles are defined by the rotation about these axes to the reference frame. While the rotation order can change, it is important to note the order of rotations. The different orders represent different intermediate frames. The combination of the rotation matrices, Equations 3.3 to Equation 3.5 create the DCM shown in Equation 3.6.

$$\left[R_x\right] = \begin{bmatrix} 1 & 0 & 0 \\ 0 & cos(\theta) & sin(\theta) \\ 0 & -sin(\theta) & cos(\theta) \end{bmatrix} \tag{3.3}$$

$$\left[R_y\right] = \begin{bmatrix} cos(\phi) & 0 & sin(\phi) \\ 0 & 1 & 0 \\ -sin(\phi) & 0 & cos(\phi) \end{bmatrix} \tag{3.4}$$

$$\left[R_z\right] = \begin{bmatrix} cos(\psi) & sin(\psi) & 0 \\ -sin(\psi) & cos(\psi) & 0 \\ 0 & 0 & 1 \end{bmatrix} \tag{3.5}$$

$$\left[R_{BodytoNAV}\right] = R_z * R_y * R_x \tag{3.6}$$

Using these rotations representing a 3-2-1 rotation, different frames can be reached by multiplying $R_{BodytoNAV}$ with the three dimensional information represented as a $3x1$ vector.

The limitation mentioned earlier about the gimbal lock of the system can be circumvented by utilizing a quaternion through different portions of the computations. Utilizing the newly defined rotation matrix, where $r_{i,j}$ represents the i row and j column component, a quaternion can be created. Equation 3.7 shows an example of one of the equations that can be used for a quaternion[11].

$$\begin{bmatrix} q_0 \\ q_1 \\ q_2 \\ q_3 \end{bmatrix} = \begin{bmatrix} (R_{21} - R_{12})/4 * q_3 \\ (R_{13} - R_{31})/4 * q_3 \\ (R_{23} - R_{32})/4 * q_3 \\ 0.5 * \sqrt{(}1 - r_{11} - r_{22} + r_{33}) \end{bmatrix} \tag{3.7}$$

There are several other forms but result in the same values. Direct forms of the translation from the euler angles to quaternions and the inverse are shown in equations 3.8 and 3.9[11]. Equation 3.8 is specific for a $3-2-1$ rotation[11].

$$\left[\vec{q}_a^b\right] = \begin{bmatrix} \cos(\phi/2) * \cos(\theta/2) * \cos(\phi/2) + \sin(\phi/2) * \sin(\theta/2) * \sin(\phi/2) \\ \cos(\phi/2) * \cos(\theta/2) * \sin(\phi/2) - \sin(\phi/2) * \sin(\theta/2) * \cos(\phi/2) \\ \cos(\phi/2) * \sin(\theta/2) * \cos(\phi/2) + \sin(\phi/2) * \cos(\theta/2) * \sin(\phi/2) \\ \cos(\phi/2) * \cos(\theta/2) * \cos(\phi/2) - \sin(\phi/2) * \sin(\theta/2) * \cos(\phi/2) \end{bmatrix} \tag{3.8}$$

$$\begin{bmatrix} \psi \\ \theta \\ \phi \end{bmatrix} = \begin{bmatrix} \arctan(\frac{2*(q_0*q_3+q_1*q_2)}{q_0^2+q_1^2-q_2^2-q_3^2}) \\ \arcsin(2*(q_0*q_2-q_1*q_3)) \\ \arctan(\frac{2*(q_0*q_1+q_3*q_2)}{q_0^2-q_1^2-q_2^2+q_3^2}) \end{bmatrix} \tag{3.9}$$

The majority of the computations in this thesis occur in a local navigation frame such as NED or ENU. ECEF positions must be converted to one of these frames to be used in the computations. Converting from ECEF to ENU requires the position of the device in latitude

and longitude defined by Φ and Λ respectively. Due to the earth not being a perfect sphere, an iterative approach must be used [30], [7]. A model for the earth is required in this process. Typically in GPS systems, the world geodetic system 1984 (WGS84) is used for this model. Figure 3.3 shows the relationship between the latitude and longitude for a specific ENU frame.

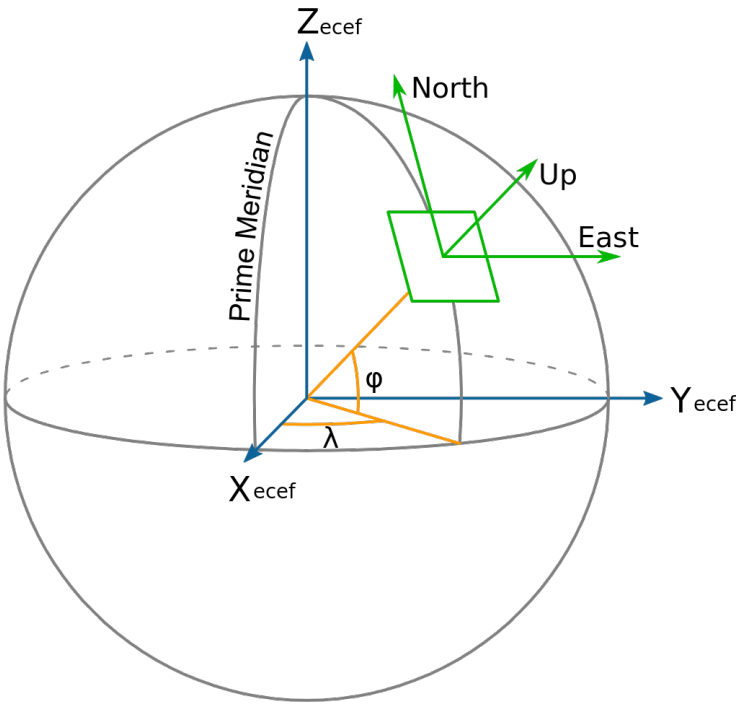

Figure 3.3: Representation of an ENU frame with respect to the ECEF frame

Using trigonometric relationships, it can be seen that these angles can be related to the origin of the ENU frame as shown in equations 3.10 and 3.11.

$$\tan \lambda = \frac{Y_{ECEF}}{X_{ECEF}} \tag{3.10}$$

$$\tan \phi = \frac{Z_{ECEF}}{\sqrt{X_{ECEF}^2 + Y_{ECEF}^2}} \tag{3.11}$$

These equations suffice for a perfectly round earth as mentioned before. To account for the ellipsoidal shape of the earth, WGS84 parameters are used. Equations 3.12 through 3.16 are used in the iterative process to calculate the latitude and longitude.

$$a_e = 6,378,137m \tag{3.12}$$

$$b_e = 6,356,752m \tag{3.13}$$

$$e_p = 3.35261 * 10^{-3} \tag{3.14}$$

$$L_{i+1} = L_e + e_p * \sin 2 * L_i \tag{3.15}$$

$$L_e = \arctan \frac{Z_{ECEF}}{\sqrt{X_{ECEF}^2 + Y_{ECEF}^2}} \tag{3.16}$$

This process is continued through longitudes to produce a sufficiently accurate result. While this can be used to convert the ECEF to latitude, longitude and altitude (LLA) . The ENU or NED frame still requires the use of a reference LLA to represent the origin of the tangent coordinate frame. This can be done at the initial point of the

3.2. Attitude Estimation

Attitude estimation using GPS varies greatly in complexity. Starting with a position solution at each antenna, the attitude can be found using large antenna baselines and calculated directly. The error on this system is directly proportional to the error of the positions and antenna baseline. Another option is to use the gps carrier signal to generate directional unit vectors of each signal over the antenna array [28]. Figure 3.4 shows a two dimensional physical representation of the wave front impinging on the antenna array from a single satellite.

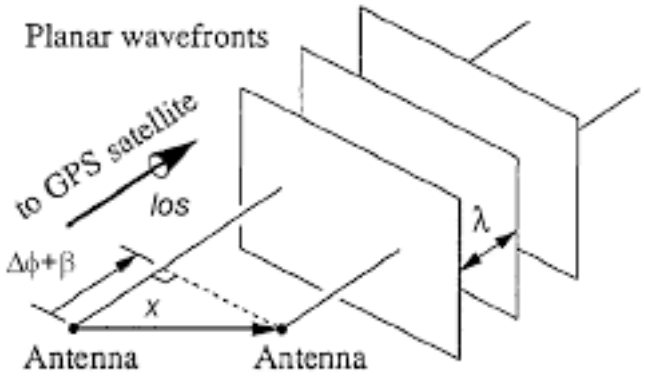

Figure 3.4: Representation of the unit vector generated by the differenced carrier phase over multi-antenna systems

Using the differential carrier phase and the known geometry between antennas allows for the satellite angle of arrival to be calculated. This is calculated by the difference in the tracked carrier phase through each antenna. This AOA estimate becomes directly dependent on CN0, baseline and actual AOA. Modeling the carrier phase as a trigonometric function can be seen in Equation 3.17 and 3.18.

$$\theta = \cos^{-}1\frac{\tilde{\Delta L}}{B} \tag{3.17}$$

$$\tilde{L} = L + \eta(0, \sigma = f(SNR, BW)) \tag{3.18}$$

This model has been shown in [7] and [34]. The noise is added to the delta carrier measurement, L while the baseline is varied to produce a ratio in order to find the angle. The noise is varied in meters to minimize the requirement for the receiver parameters to be defined. The receiver carrier noise is dependent on the devices tracking loop [44],[29] and [34]

Figure 3.5 shows the error of several baselines with respect to various noise levels.

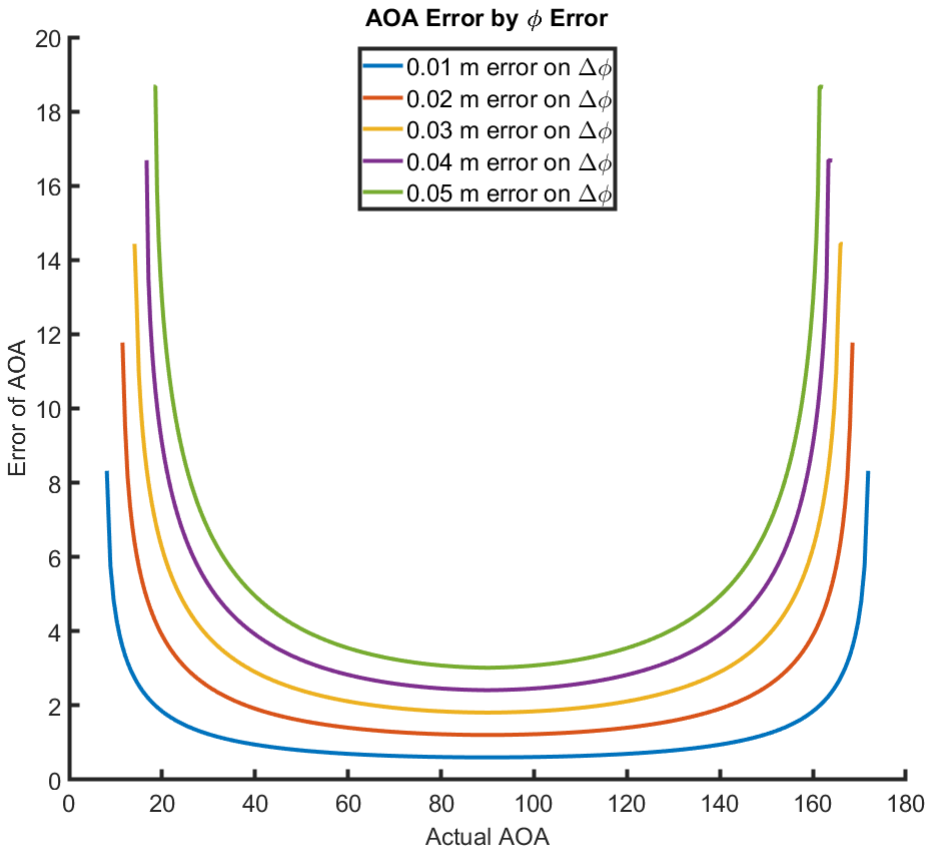

Figure 3.5: CW AOA Error with respect to Elevation and Measurement Error

The relationship between the expected and actual AOA while considering the baseline shows higher antenna separation results in lower AOA error. Extending this figure across a single noise level of $0.05m$ on $\Delta\phi$ results in figure 3.6.

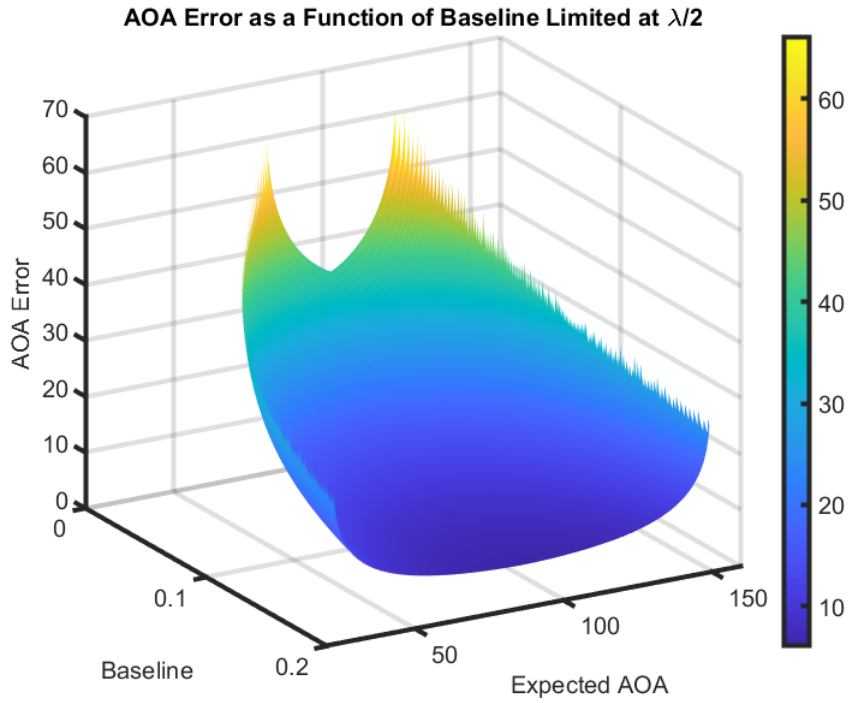

Figure 3.6: CW AOA Error with respect to Elevation and Antenna Separation

From this figure we can see that at the shortest baseline (0.02m), the AOA error is much higher. This is because the differential carrier noise, ignoring clock error due to measurements having a common clock, is a larger ratio of the baseline. This is why the error increases as the baseline get smaller. The same result can be seen as the angle approaches the horizon ($0\,\text{deg}$,$180\,\text{deg}$). In each case, the noise results in a larger ratio of the measurement or can be described as a decreased signal to noise ratio (SNR).

Using the modeled measurements, an attitude simulation can be created using this to generate the signal noise errors. The system estimates three states for an instantaneous attitude estimate. The roll pitch and yaw are estimated using both nonlinear least squares and an extended kalman filter. Equations 3.19 represents the measurement model while Equation 3.20 and 3.21 represent the observation equations.

$$\hat{y} = b_i^T * A(\hat{X}) * A_E^R * \hat{S}_j \tag{3.19}$$

$$\hat{y} = H(\hat{X}) \tag{3.20}$$

$$H = \begin{bmatrix} \frac{\partial h_1^1}{\partial x_1} & \cdots & \frac{\partial h_i^1}{\partial x_l} \\ \vdots & \ddots & \vdots \\ \frac{\partial h_1^j}{\partial x_1} & \cdots & \frac{\partial h_i^j}{\partial x_l} \end{bmatrix} \tag{3.21}$$

Table 3.2 defines the parameters in these equations.

Table 3.1: Estimation Equation Variables

Parameter	Size	Description
b_i	$1x3$	Body vector from antenna one to antenna i
$A(\hat{X})$	$3x3$	DCM using current attitude estimates
A_E^R	$3x3$	DCM rotation from ECEF to Reference
$\hat{S}_j$	$3xN$	Directional unit vector to satellites one to j
$\frac{\partial h_i^j}{\partial x_l}$	$1x1$	Partial derivative with respect to state l, sattelite j, and antenna i

Equation 3.19 represents the projection of the body frame satellite unit vectors onto the antenna array in the body frame for each satellite. This equation results in fractional wavelengths or meters of the signal and should be accounted for appropriately as the only units in the equation are from the antenna vector b_i.

Utilizing the combination of these equations, a GPS attitude based system can be simulated. In each system, the system is simulated with dynamics limited to a single state at a time to retain simplicity. Figure 3.7 shows the results of the NLS estimation and figure 3.8 shows the error.

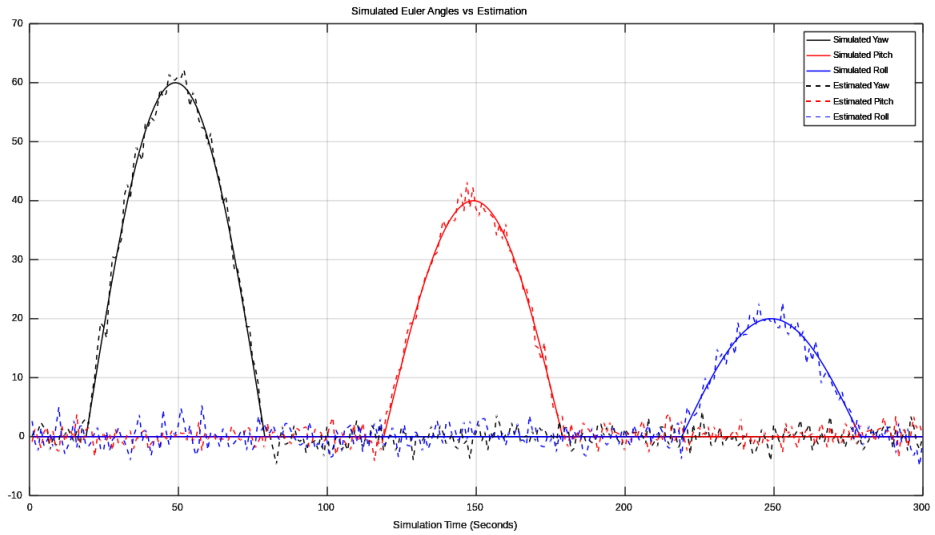

Figure 3.7: Non-linear Least squares attitude simulation

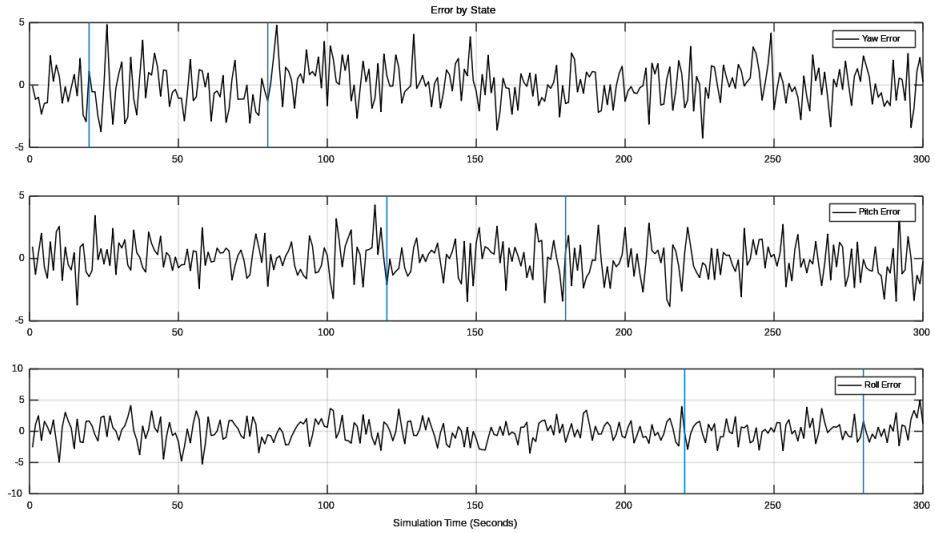

Figure 3.8: Non-linear Least squares attitude simulation error and showing the dynamic bounds

The error plots show vertical lines where the dynamics start and end in each rotation. Each individual attitude solution is simulated and solved with eight satellites, average CNOs of 42 and a baseline of 0.9λ.

The Non-linear solution produces sufficient results and can be improved. A kalman filter can benefit from the past information. The simulation shows a slight phase lag in the kalman filter suggesting that it is filtering too much of the signal. In low dynamic periods, the filter

outperforms the NLS by a couple degrees in each rotation. Using equations 3.22 to 3.26 and simulating a chosen baseline from figure 3.5 an attitude system can be simulated.

$$\hat{X}_k^- = A * \hat{X}_{k-1} + B * U \tag{3.22}$$

$$P_k^- = A * P_{k-1} * A^T + Q \tag{3.23}$$

$$K_k^- = P_k^- * H^T * (H * P_k^- * H^T + R)^{-1} \tag{3.24}$$

$$\hat{X}_k = \hat{X}_k^- + K_k^- * (Z_k - H * \hat{X}_k^-) \tag{3.25}$$

$$P_k = (I - K_k * H) * P_{k-1}^- \tag{3.26}$$

The results are shown in figure 3.9 and 3.10.

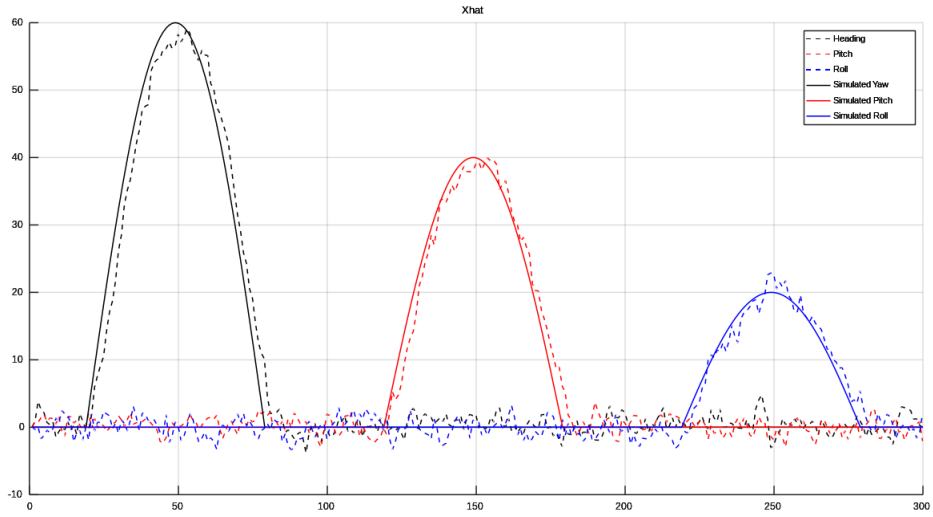

Figure 3.9: EKF attitude simulation

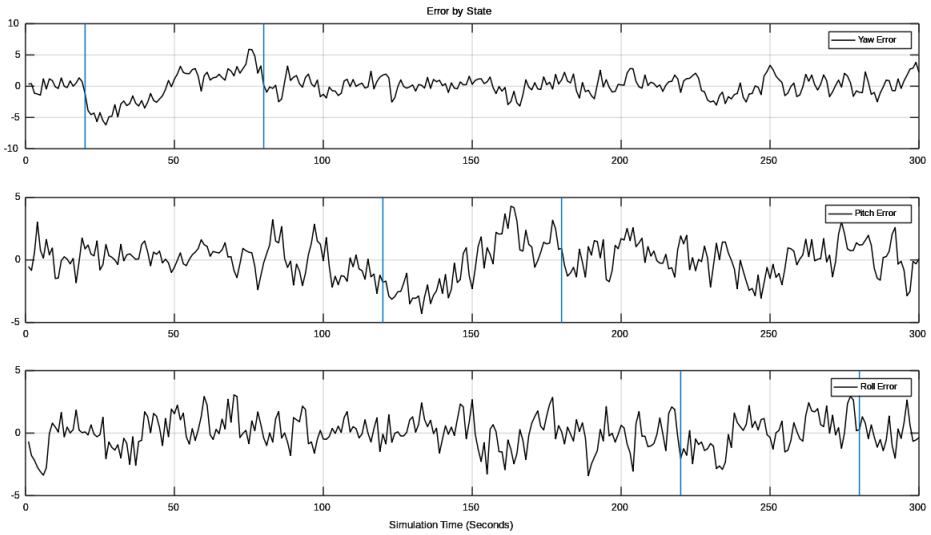

Figure 3.10: EKF attitude simulation error

Completing a Monte Carlo Analysis on the attitude results of the differential carrier phase, it can be shown that a system with a static baseline and receiver parameters results in an improved attitude estimation at longer baselines [13, 10, 7, 27]. Figure 3.11 shows the expected attitude error from GPS as a function of antenna distances. This assumes using only one datum antenna and no cycle slips in the system.

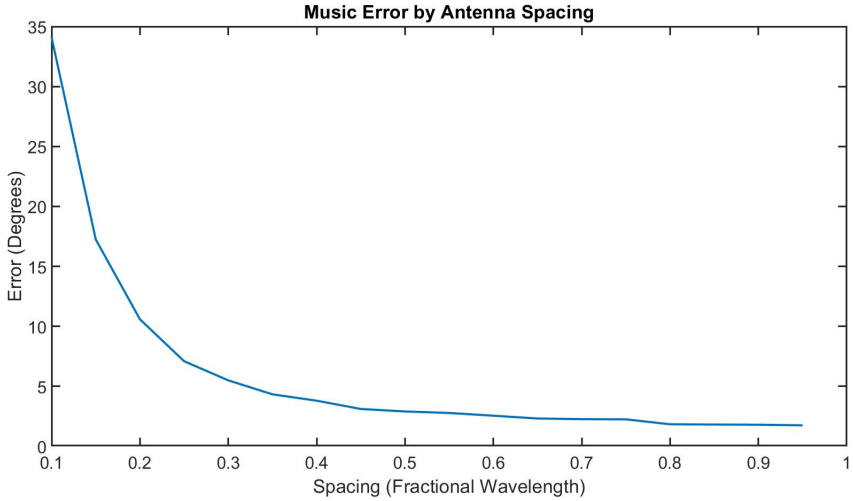

Figure 3.11: MUSIC Error over various Antenna separation

3.3. Positional Noise affects on attitude

It is important to note that the distance between the antennas d, must be larger than the positional noise variance to prevent large errors in the attitude measurement. In the event of two noisy positions of the antennas, the noise added can cause the vector to change directions causing the resulting solution to have a large error. This is easier seen in the two dimensional case when considering heading. Note, the two dimensional case does not consider altitude of the antennas.

In the two dimensional case, heading is the observable rotation. The position solution of each antenna is solved independently, then differenced. This type of solution is synonymous with the pseudorange positioning method. The differenced result is the heading vector. The true heading is measured from the positive y-axis of the reference frame to the true differential position vector as shown in figure 3.12. The measured differential position vector is shown as a dashed line. ψ represents the heading and measured heading in both figures 3.12 and 3.13.

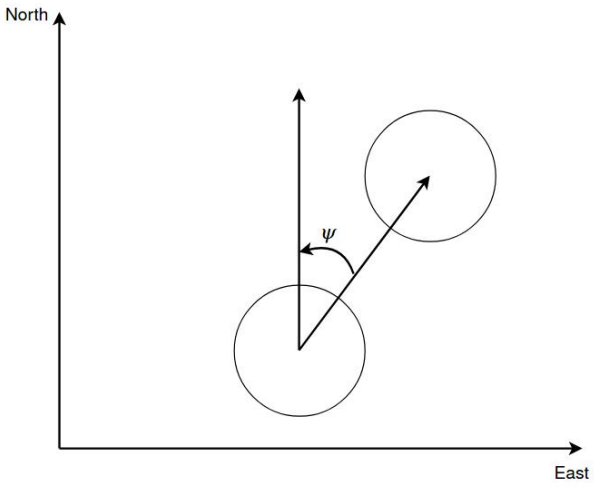

Figure 3.12: True heading with potential position error of each antenna

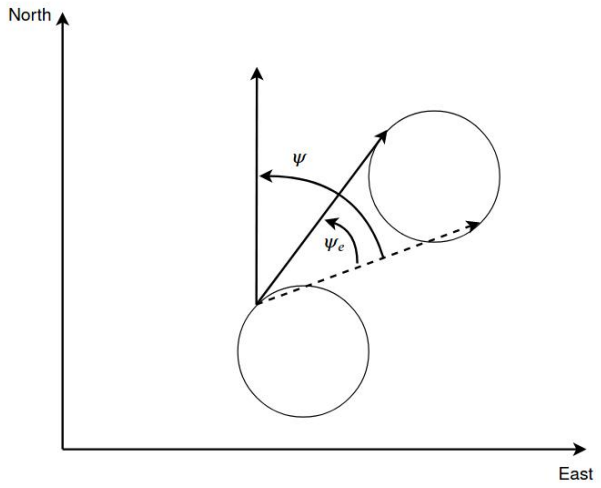

Figure 3.13: Measured heading with potential position error

The subscript e represents the the error of the measured vector with respect to the true vector. The circles represent the three sigma bound of the position of each antenna. From this it is easy to see the potential error of the measured heading vector as in figure 3.13. These figures show the appropriate distances between antennas. When the antenna distance is smaller than the potential error and the potential errors overlap, the vector can invert and cause the measurement to have large errors. Figure 3.14 shows this scenerio.

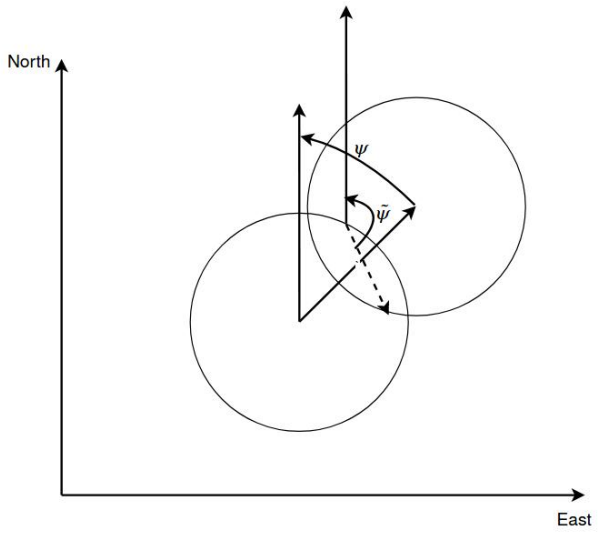

Figure 3.14: Measured heading with short antenna separation

This noise overlap is applicable to the pseudorange and carrier phase positioning methods. Each positioning method has a noise level associated with it but are orders of magnitude different. The measured angle error is proportional to the three sigma value and inversely proportional to the distance between the antennas. Each are evaluated separately due to the noise limitations of each solution. This is the lower limitation for the baselines for each pseudorange and carrier phase methods.

Chapter 4 Angle of Arrival Estimation

The angle of arrival (AOA) refers to the direction that a signal is coming from relative to an antenna array. The AOA can be found using signal correlation or time differences of measurements. These are the two most common methods in direction finding across an antenna array. The methods are dependent on knowing the antenna separation and having simultaneous measurements at each antenna. The signal algorithms are better suited for stronger signals relative to the noise floor (SNR), as with many other algorithms. Each method suffers from ambiguities due to the trigonometric relationships in the array and the signal. The ambiguities can be mitigated with the addition of extra antennas, which increases observability but also the required processing needs. Antenna Array size, Antenna separation, signal power, signal type and sampling times affect the results. Deriving a measurement variance for the AOA estimation is a long process which only provides a single combination of scenarios that pertain to the environment.

4.1. Signal Model

The signal model utilized for estimation of real data is dependent on several factors. some of which are antenna separation, center frequency, and the speed of light. Figure 4.1 shows a signal source emitting a signal from the far field.

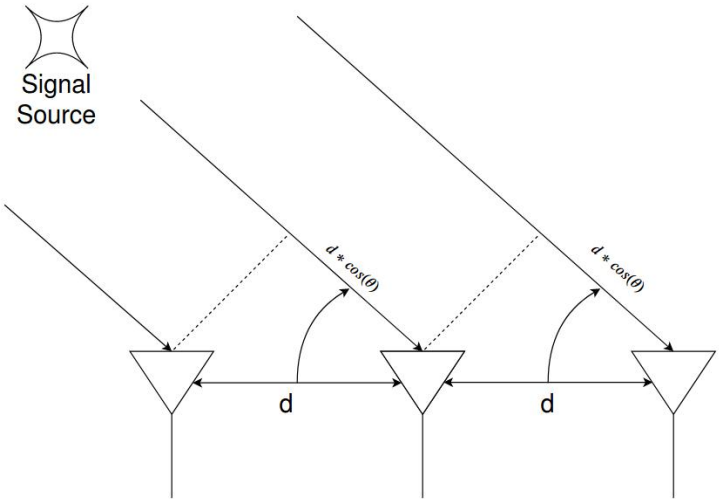

Figure 4.1: Two-Dimensional Wavefront of a Signal from a given AOA

As it approaches the antenna array. The signal is seen as a flat wave front due to the far field propagation. The far field is defined by equations 4.1 through 4.3 where r represents the range between the receiving antenna and the transmitting antenna, λ represents signal wavelength and D represents the largest dimension of the antenna, or the largest distance between any two elements.

$$r >> 1.6 * \lambda \tag{4.1}$$

$$r > \frac{2 * D^2}{\lambda} \tag{4.2}$$

$$r >> 5 * D \tag{4.3}$$

Figure 4.2 shows the physical representation of these values.

In many cases, these do not impact the ability of the estimation algorithm due to most cases that this can be applied for are at much greater distances than the far field limit. At the L1 frequency, the range is on the order of meters so localization does not provide much use when the source of the signal is within arms reach.

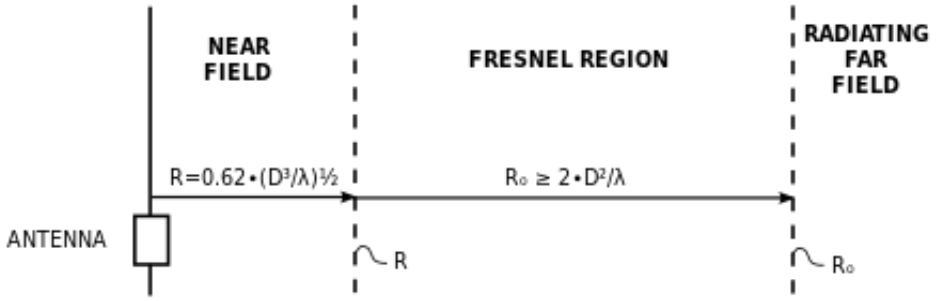

Figure 4.2: Farfield criteria

The receiving antennas are separated by some distance 'd' and due to the angle theta the signal wave front arrives at each antenna at different times. The effective delay distance is shown by the trigonometric relationship between antenna spacing and the angle theta. When theta is found to be at ninety degrees (Array broadside), the effective delay is zero and similarly, when theta is at zero degrees, the delay is proportional to the distance between antennas. When the array is receiving signals from different geometries, the delays are used in estimating the direction. When there is an ambiguity to the direction it is typically due to a mirroring of some component due to the trigonometric terms within the signal model.

Deriving the model from this image is begins by stating the measured signal is a function of the signal and some noise component. The received signal is represented by $s(t)$ in Equation 4.4 and η as the unique noise figure for each receiving antenna.

$$x_1(t) = s(t) + \eta_1 \tag{4.4}$$

This represents the signal at the base antenna. Each following element in the array has a phase offset relative to the reference antenna array element Equation 4.5 shows this relationship for each additional antenna delay in the planar, one degree of freedom case.

$$\mu_m = (M-1) * d * sin\theta \tag{4.5}$$

Here, d represents the distance between the antennas of the linear array as shown in 4.1. The trignometric term inside the delay component, Equation 4.5, is a function of the true receive

angle of arrival. Using this equation in the complex signal representation results in Equation 4.6.

$$x_m(t) = s(t) * e^{(-j*2*\pi*\mu_m)*\lambda^{-1}} + \eta_m \tag{4.6}$$

This equation shows to be a function of the signal, noise, AOA, wavelength, antenna, and element separation. Combining equations 4.4 and 4.6 for the linear array into matrix form results in the matrix Equation 4.7.

$$\bar{X_s} = \begin{bmatrix} x_1(t) \\ x_2(t) \\ \vdots \\ x_m(t) \end{bmatrix} = \begin{bmatrix} 1 \\ e^{-j*2*pi*d/\lambda*sin\theta} \\ \vdots \\ e^{-j*2*pi*(2-1)*d/\lambda*sin\theta} \end{bmatrix} * s(t) + \begin{bmatrix} \eta_1 \\ \eta_2 \\ \vdots \\ \eta_m \end{bmatrix} \tag{4.7}$$

This definition represents the signal received at each antenna with a phase delay based on the array geometry. Remaining a function of the same variables but now representative of an array.

This matrix form is useful in array processing for the subspace based methods shown later. The matrix multiplied by the base signal is commonly referred to as the array response. The array response is a starting point for beam forming algorithms and other array processing methods as many use it to define the initial values that need to be weighted to have a controlled response. It is also important to note that the noise on each element is unique. If the noises are not unique, the signal processing methods shown in this research break down due to the subspace based methods not being able to differentiate between the common signal components from element to element. While this format only shows the one DOF model, the two DOF model can be derived using the approach but utilizing the second angular measurement with respect to the array in the spherical coordinates.

4.2. Antenna Model

The signal model defines the signal as it approaches the array. The array should be defined in the physical world in the same fashion. Some signals behave differently due to polarizations

and signal structures. It is important to understand the way the array interacts with the signal before the signal is quantized on the ADC. In many cases, manufacturers of arrays will provide the necessary data to account for these errors. Power and phase errors are introduced in every antenna. Due to the antenna not being perfectly designed and manufactured. In most systems, a single antenna error has negligible impact on the system as a whole. In the case of direction finding, the array response across all combinations of angles and desired frequencies should be understood to be able to effectively find the AOA. For each antenna, the sensitivity of each of the parameters can be derived and has been well researched from Maxwell's equations[23]. The reader is directed to [19, 23] for further reading on the topic. A moderate understanding of the electric field allows for the polarization mismatch and phase error to be understood. A physical representation of the signal in the electric field can be seen in figures 4.3 and 4.4 where each arrow from the z-axis represents a vector indicating the phase and amplitude for that phasor[2].

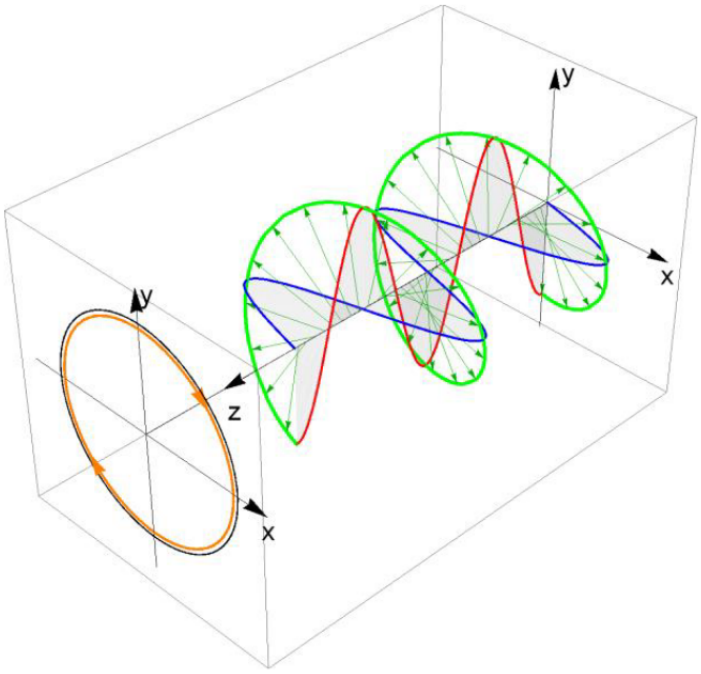

Figure 4.3: Right hand circular polarized wave propagation

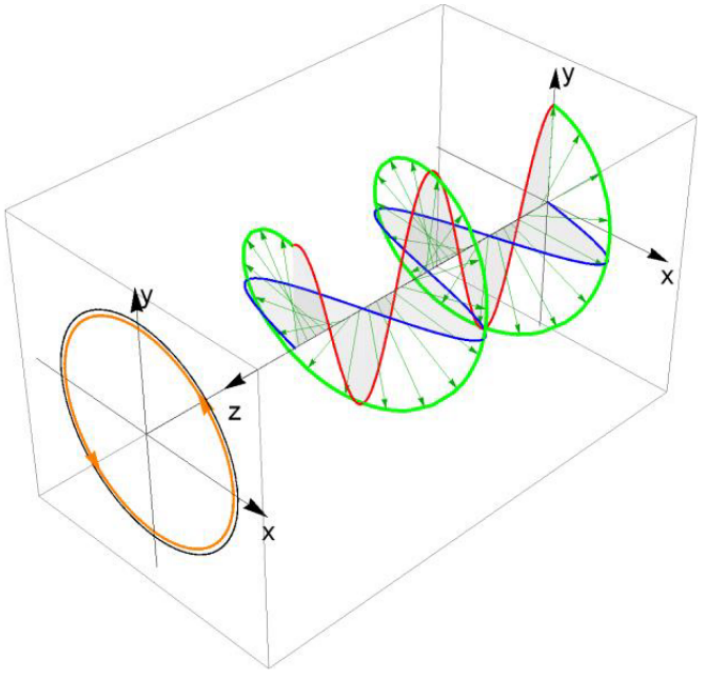

Figure 4.4: Left hand circular polarized wave propagation

A phasor references the magnitude and phase of a signal at a given instant. These figures show perfectly circularly polarized signals, not typically seen in satellite signals due to atmospheric errors[35, 23] among many other errors. While good polarization matches are common perfectly received polarization matches are difficult to achieve. The polarization similarity of the signal to antenna affect the received power past the antenna. Due to many of the algorithms using both power and phase to estimate the antenna AOA, the polarization must be considered as well. [32]. If these values have biases or nonlinearities, the AOA results will be skewed with dynamic biases. The receiving system can be calibrated to account for this offset. The polarization difference between the signal and the antenna is called polarization mismatch. Equation 4.8 shows the relationship between received signal power and transmit power with various coefficients pertaining to the polarization and circuit components.

$$P_R = p * q \frac{P_T * G_T * G_R * c^2}{4^2 * \pi^2 * d^2 * f^2} \tag{4.8}$$

Variable p represents the polarization mismatch, restricted between zero and one which directly scales the receive power. Impedance mismatch is q. P_R and P_T are receive and transmit

power respectivly. G is gain. d c and f are distance, speed of light, and frequency of the signal, respectively. The wave propagation, polarization and rotation of the signal all impact the received signal through any given antenna. These are all factors that should be considered when designing any electromagnetic direction finding system.

As these figure show a perfectly polarized signal, the projection of the tip of the vector onto the x-y plane shows the polarization shape. This is ideally a perfect circle. On the Poincare sphere shown in figure 4.5, all potential polarizations of signals are shown. In this case, the two signals shown are at the top and bottom of the sphere representing left and right circular polarization.

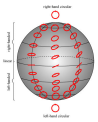

Figure 4.5: Poincare Sphere

In practice the signal is not perfectly located at the point desired. Addressing polarization errors can be done in the front end processing as part of a calibration utilizing the manifold data typically given by the antenna manufacturer.

4.3. Multiple Signal Classification

Multiple Signal Classification (MUSIC) utilizes the signal and noise subspace based eigen value decomposition of the covariance matrix for direction finding. The algorithm has been heavily research over the last fifty years by various groups with defense companies making the largest strides with the algorithm initially[4]. Accounting for all antenna spacing and iterating the algorithm over the array response search space allows the observer to find a direction in which the maximum power is received by an antenna array. This is the AOA with respect to the antennas coordinate frame. Each antenna observes unique noise and the signals present in the environment. The noise for each antenna is generally uncorrelated. The received signal is correlated because they originated from the same transmitter, ideally and ignoring the possibility of multipath. Mutual coupling of antennas can cause issues in the measurements received,

however it is assumed the associated errors are properly calibrated for in this thesis. As they are commonly given in manifold data or this data can be generated in an anechoic chamber over all operational parameters and directions of the antenna array. Defining the covariance matrix and what is represented is important for these assumptions as well as in determining the signal results and values. A covariance matrix is the CRPA's received signals multiplied by itself. This creates a square matrix of size NxN, where N is the number of antennas in the array. This matrix is composed of complex values and squared complex values on the diagonal which results in only real terms. The magnitude of each signal can be found from the covariance diagonal. The remaining phase components can be measured with respect to a reference element. There are several other factors that also play into the covariance matrix such as dwell time (sampling time), number of samples used (number of quantized values to average). This matrix contains many different noise sources and is very difficult to model perfectly. Table 4.1 shows the current list of assumptions and its source and if it is unique to the element or array.

Table 4.1: Noted Noise Sources

Noise	Source	Note
Thermal Noise	Antenna	Unique to each antenna design
Clock	System Oscillator	Unique to each antenna system clock
Quantization	ADC	Unique to each RF path
Local Oscillator	Drving timing oscillator	Unique to each down conversion system
Bias Estimation	System channel estimation algorithm	unique to each calibration

Making and continuing with these assumptions allows the AOA to be found from the correlation matrix as shown in Equation 4.9 where H represents the hermitian transpose of the complex signal matrix[12].

$$R_{xx} \approx E[\bar{X} * \bar{X}^H], where \bar{X} = [s(t)_1 ... s(t)_n] \tag{4.9}$$

As the complex vectors grow, the accuracy of the direction estimate increases. Equations 4.11 and 4.10 show the representative model holding all previous assumptions true.

$$R_{ss,ij} = E[s(t)_i * s(t)_j^H] \tag{4.10}$$

$$R_{xx} = A * R_{xx} * A^H + \sigma_N^2 * I_M \tag{4.11}$$

A represents the geometry relationship of the antennas based on the signal delay as shown in Equation 4.7. σ represents the collective noises from 4.1 lumped into one term.

Equation 4.11 is sufficient for simulation but is not useful for application as the true signal level is not known. In real time applications. R_{xx} is estimated by making assumptions of the stochastic characteristics of the system to be replaceable by the expectation. Equation 4.12 shows the relationship of real time samples to the signal correlation matrix estimate.

$$R_{xx} \approx \hat{R_{xx}} = \frac{1}{N} * \sum_{i=1}^{N} x(t) * x^H(t) = \frac{1}{N} * \bar{X} * \bar{X^H} \tag{4.12}$$

Using the array response matrix, the conventional MUSIC equation is formed by using the response matrix and signal matrix. The combination of these two produce an equation as a function of the AOA. This equation, for the linear array, is used as a search space to find a maximum power in a specific direction. Equation 4.13 is the conventional form of MUSIC in the one DOF system.

$$P(\theta) = \frac{A^H(\theta) * \hat{R_{xx}} * A(\theta)}{A^H(\theta) * A(\theta)} \tag{4.13}$$

Equation 4.13 results in a relative signal power with respect to the receive signal power. As the search space is indexed, the power level will reach a peak. At this point, the signal delay according to the array response is in the direction of the signal and is representative of

the impinging signal direction. This angle is the AOA estimate. Modifying the equations to a two dimensional system is simple process of adding another dimension to the equations from the linear equations. Starting from Equation 4.5 the equation is modified to create a single response for each antenna. The resulting equation is shown in Equation 4.14.

$$x(t) = A_i * \exp^{\frac{-j*2*\pi}{\lambda} * \begin{bmatrix} dx & dy & dz \end{bmatrix} * \begin{bmatrix} \cos(\theta) * \cos(\phi) \\ \sin(\theta) * \cos(\phi) \\ \sin(\phi) \end{bmatrix}} \tag{4.14}$$

The terms dx,dy and dz are the Cartesian differences of the antennas from the reference antenna. θ and ϕ are the azimuth and elevation angles of the search space. The physical representation of these angles are shown in figure 4.3.

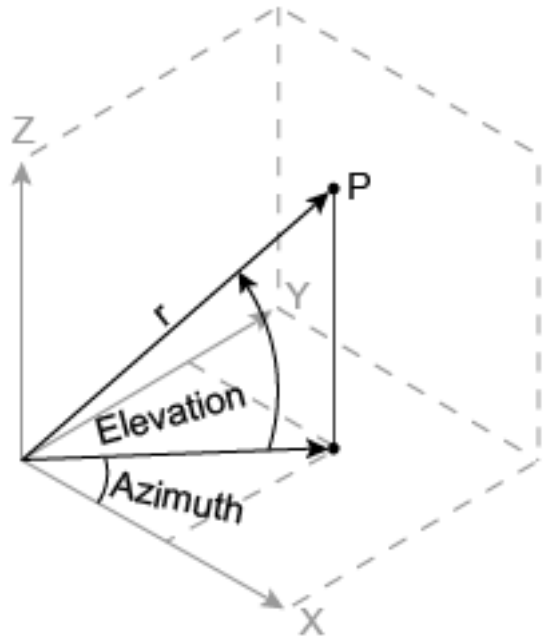

Figure 4.6: Azimuth and Elevation Physical Representation

The remaining equations for $\bar{X}(t)$ and R_{xx} are extended to include all antenna combinations with the reference antenna. As for the MUSIC equation in 4.13, it is extended by iterating over a larger steering array. This increases computation time significantly. Equation

4.15 shows the resulting equation where each component is derived using the antenna response from Equation 4.14.

$$P(\theta,\phi) = \frac{A^H(\theta,\phi) * R_{xx}\hat{(}\theta,\phi) * A(\theta,\phi)}{A^H(\theta,\phi) * A(\theta,\phi)} \tag{4.15}$$

Defining the error of the algorithm is not a simple solution due to the many parameters that play a role in the estimate. Monte Carlo simulations were used to estimate the expected error in a given direction over various signal powers and white noise bandwidths. The Monte Carlo results of the music algorithm are shown in figure 4.3 for a single bandwidth and direction.

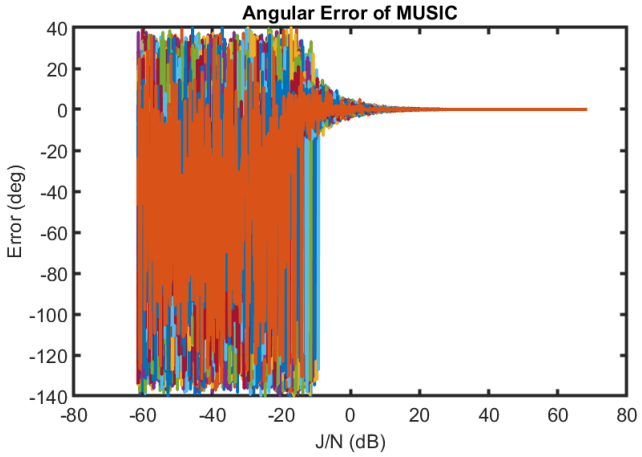

Figure 4.7: Monte Carlo Music Simulations

The simulation uses the same parameters as the shown in table 4.2.

Table 4.2: MUSIC Parameters

Parameter	Value
Antennas	4
Array	Planar
Frequency	1575.42 MHz
Samples	2500
Spacing	0.2 * λ m
SNR	-25:10 dB
Signals	1
Signal Type	AWGN
BW Ratio	0.05:1

This particular portion of the simulation shows the error for a single AOA. As the signal approaches the noise floor threshold (0 dB), the error of the signal dramatically reduces. At a SNR of zero, the error can be seen to be contained to within a few degrees of truth. On certain combinations of platforms and signals, this is the point where navigation signal quality received can be seen to diminish. These are the minimum signal levels that have a chance of changing a GPS receiver's tracking ability. At this point the ability to localize the signal becomes much greater. To completely inhibit the receivers operation, the power must be significantly higher but is dependent on the receiver's operation to define a lower limit to hinder the receiver completely.

Using the same information across all Monte Carlo simulations, the expected error of a white noise interference signal at the antenna center frequency is shown as a function of Signal to Noise ratio and signal bandwidth relative to the front end bandwidth. Figure 4.3 shows the absolute error of this particular combination of signal and array at random azimuth directions.

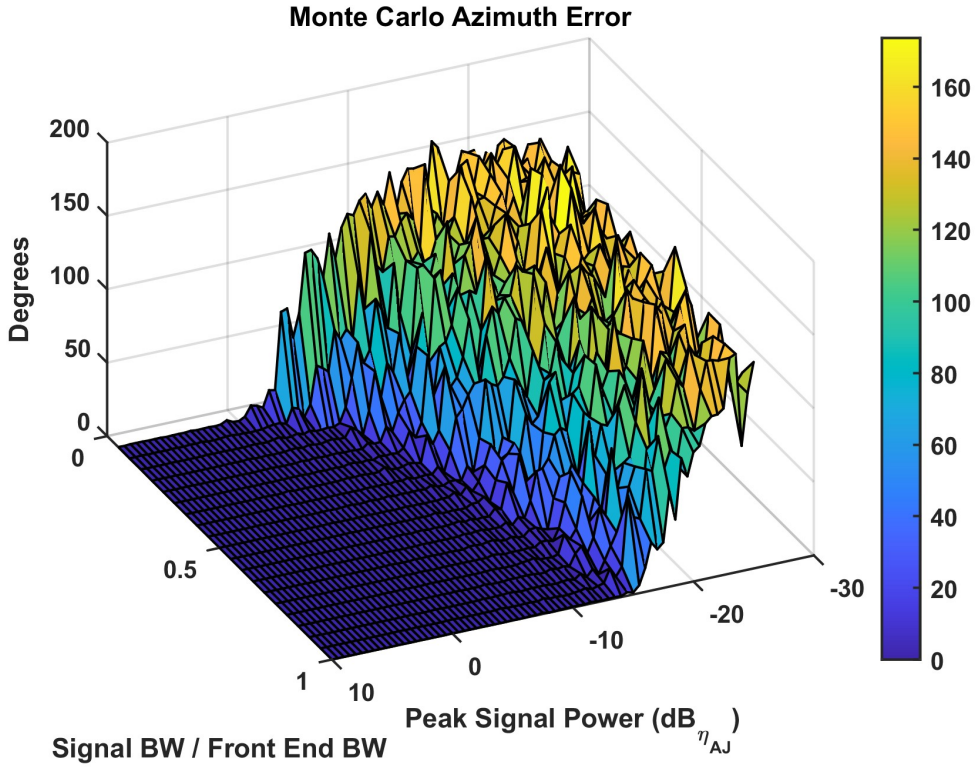

Figure 4.8: Monte Carlo mean azimuth error

Figure 4.3 shows the elevation error over the same simulation.

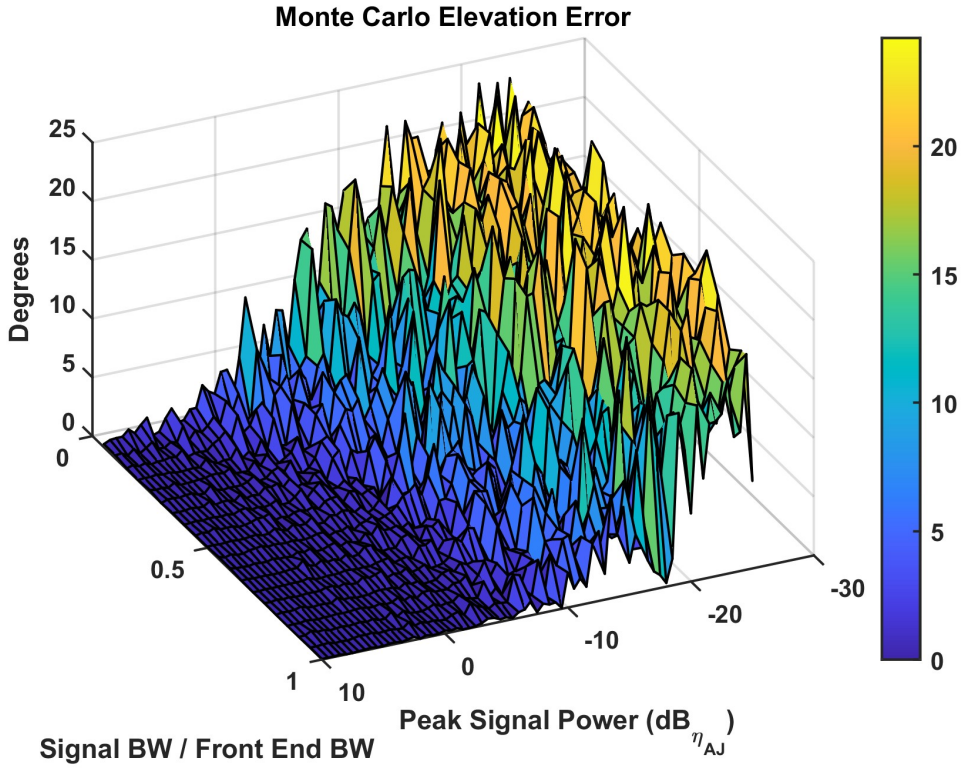

Figure 4.9: Monte Carlo mean elevation error

These give general trends for the relationship of the algorithm using an example set of idealized antennas. Although other solutions such as dual polarization antennas are capable of producing the azimuth of a known signal but at a much higher uncertainty[26], other multi-element methods are more accurate. As seen with using a CRPA, when the signal is above the noise floor, MUSIC or signal phase differencing are capable of finding these directions effectively. The azimuth and elevation error show that as the signal power is increased the error on the directional measurement reduces quickly. The slant in error reduction away from the noise floor is due to the signal power being spread across a bandwidth. As the power spreads, the peak power drops. This drop is adjusted to maintain a steady peak power across the all simulated bandwidth. Combining these errors into a value encompassing the entirety of the error, the angular error was used to compute a RMS error between the two angles. this shows a similar error curve over the same simulation in figure 4.3.

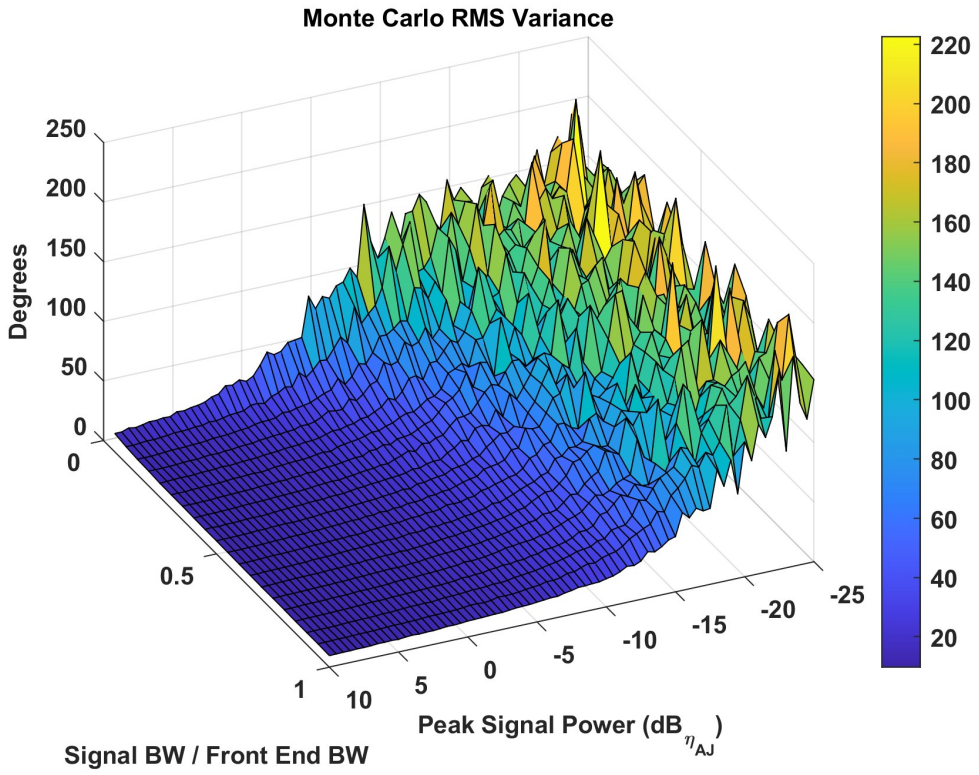

Figure 4.10: Monte Carlo mean RMS error

As these curves are observed, a relationship to the eigenvalues of the covariance matrix during the music estimation and rms error can be seen. Figure 4.3 shows the plane of eigenvalue averages for each antenna during the same simulation.

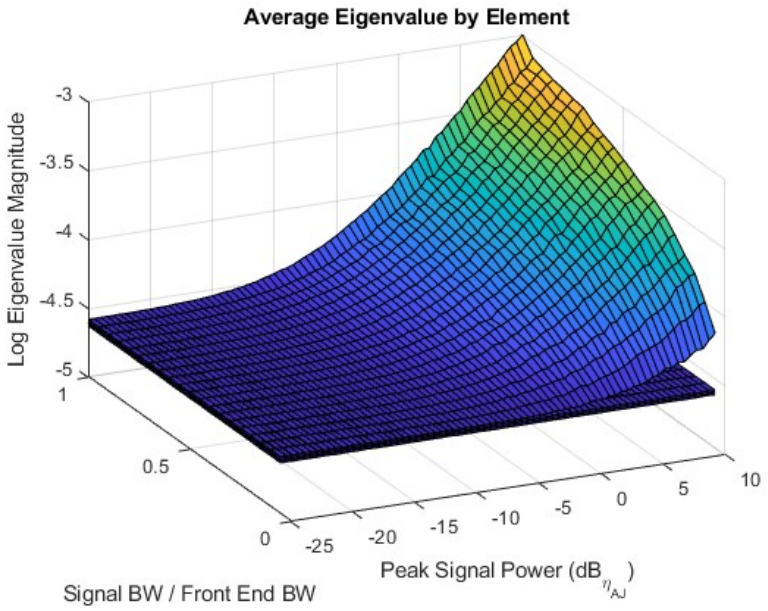

Figure 4.11: Monte Carlo mean RMS error

It is obvious to see as the signal power increases and bandwidth increases, the eigenvalue of one antenna separates itself from other antennas. This eigenvalue is represents the eigenvalue representing the signal subspace. It is important to note the axes are flipped in this image to allow visibility of the eigenvalue plane.

Chapter 5 Radio Source Localization

Localization of a signal source requires a combination of different types of information, including positions, attitudes bearings and ranges. When combining these, it is commonly known as a form of triangulation, trilateration or multilateration. Triangulation refers to geometry based point deduction, typically from bearings at two known points. Given the nature of the measurements available and unknowns of the signal of interest, triangulation will best fit the needs of this problem. The methods utilized here, focus on a combination of position, attitude and bearings. While range can still be used as an aide to these methods, it requires assumptions that can only be estimated after localization or from other forms of estimation.

A single moving platform can identify and localize a single source that is stationary [32] and even a non-stationary target given dynamic requirements are met [32, 31]. This requires additional tracking states and a different coordinate frame to assist the filter in stability. More can read on this topic in [31]. The platforms maneuvering and navigation capabilities directly impact the capability of the device to localize a source. Lack of positional diversity reduces observability of the point of interest while positional error adds proportional positional error to the final estimate. Since the range to the device of interest is unknown it is difficult to define the error on the target location based on this unknown range and angular measurement relationship. This is one of the difficulties of the problem of localizing a source using bearing only measurements.

There are many ways to create an estimate of a source location given only bearing measurements. Looking at purely geometric solutions is an option, especially when diverse angular measurements are provided. Over the course of an extended period of measurements, the (approximately) zero mean angular measurement should be able to create a rough estimate of the source location through an averaging of the points provided by the triangular geometry created

from the bearing measurements. Different formulations of the vertices created by the bearing intersections have different names such as centroid, in-center or bisector[32]. These are common formulations of purely geometric solutions to the problem.

More standardized estimation methods such as least squares and kalman filtering provide the opportunity to account for the noise in the system. Using the AOA as a measurement also requires some knowledge of the noise of the front end system due to the inconsistent power received inherently in this problem. AOA noise, as shown previously is heavily dependent on the system parameters defined by the designer, and should be adapted for through subspace or signal processing methods.

To compare these methods, the source estimate location error can be measured by deterministic methods such as root mean square error (RMSE) or circular error probable (CEP). RMSE is the magnitude of the vector from the estimate to the truth. CEP describes the area that defines the probability of the truth being contained in the area enclosed. This probability threshold can be any chosen percentage but is commonly depicted as fifty or ninety-five. To assist in the understanding of these comparisons, Crao Ramer lower bound (CRLB) defines the reference for the ideal statistical estimate. The CRLB is an upper bound on the error covariance matrix for an unbiased estimate[32]. Quantifying the error is done with CEP or RMSE. Showing these values along with the CRLB for the same iterations show the 'inefficiency' of the estimation solution.

5.1. Measurement Generation System

The localization methods described still require accurately modeled or simulated measurements. The generation of these measurements in hardware would be much simpler process if creating an interference signal was legal. In lieu of an adequate operational area, an open hardware in the loop system was created. Creating an open loop hardware system to get beyond just simulation is one of the few options available to have these measurements. While hardware in the loop systems are not always perfectly representative of real scenarios, they do provide enough accuracy for system understandings if calibrated appropriately.

This particular system requires a less common technology, the RF delay system capable of resolutions in the pico-second time frame for each antenna. Other portions of the system such as ettus research devices are more common and are commonly used to generate and receive signals. The remaining subsections are commonly used in industry and can be found in many places. Combining these types of hardware to create the system was achieved through several networked devices to create an inexpensive small scale wave front simulation system(Relative to commercial wave front GNSS simulation systems). Table 5.1 shows the list of devices used to create and control the wavefront simulation.

Table 5.1: Measurement Generation Hardware

Device	**Use**
Rackmount desktop	software host and interface
USRP N310	Phase delayed signal reception
USRP N210	Signal Generator
USRP N210	Local Oscillator
JFW RF Attenuation	Signal conditioning
Gigabaudics QAPDL-5	Signal phase delay
Raspberry Pi 3	Phase delay controller

Figures 5.1 through 5.3 show the physical hardware and connections.

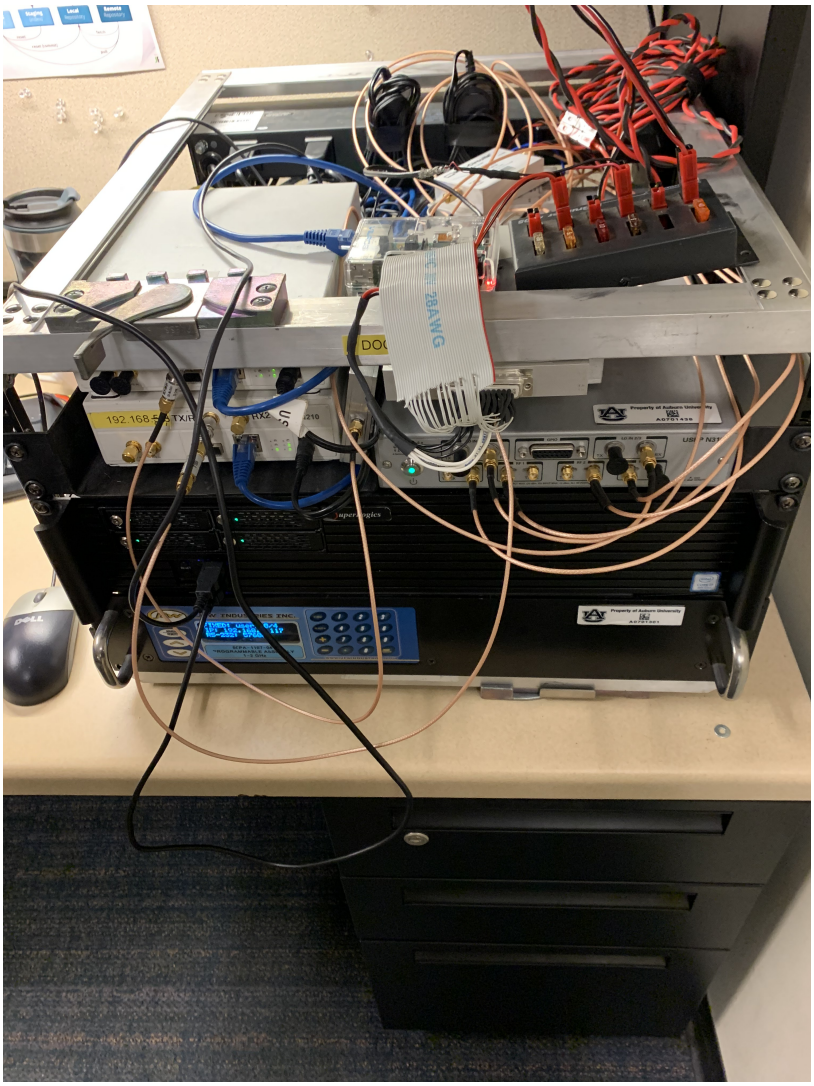

Figure 5.1: HWIL system (Front)

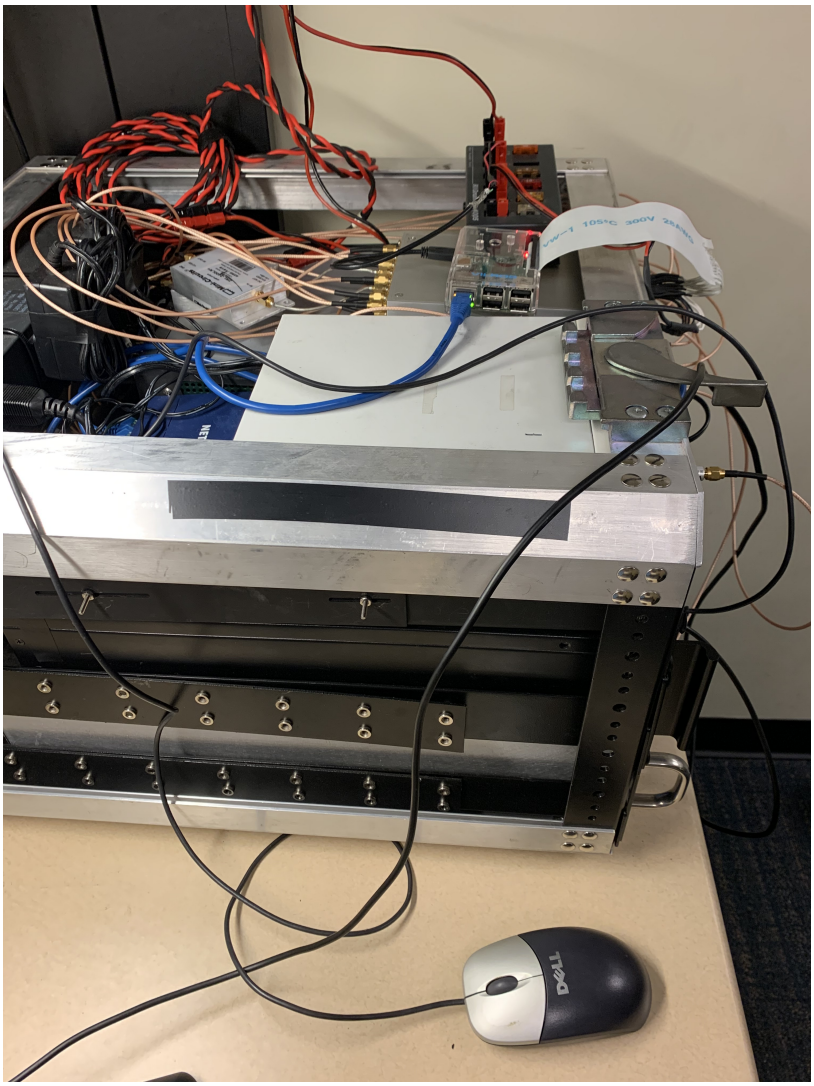

Figure 5.2: HWIL system (Side)

Figure 5.3: HWIL System attenuation

The ettus devices handle all signal generation and reception. The signal power and timing is controlled by the raspberry pi using the GPIO pins as inputs to the gigabaudics phase delay system. Interfacing with each of these required their own software to interface and time align the systems. Table 5.2 shows the list of software used in the measurement generation process.

Table 5.2: Measurement Generation Software

ROS	**GNURadio**	**UHD**	**Other/Custom**
Navigation Filter	AOA Estimation	LO Generation	Localization Filter
Planned Path	IQ Calibration	Signal Sampling	Initial Estimates
Emitter Location	Clock Calibration	Signal Generation	Phase Delay
Signal Type	Signal Model		Timing
MUSIC Parameters	AOA Model		

These software systems include Robot Operating System (ROS), USRP Hardware Driver and GNURadio. These are relatively common software systems that handle the hardware interactions and timing. To aide in creating a full description of the simulation system figure 5.1 shows the flow of information in the the simulation.

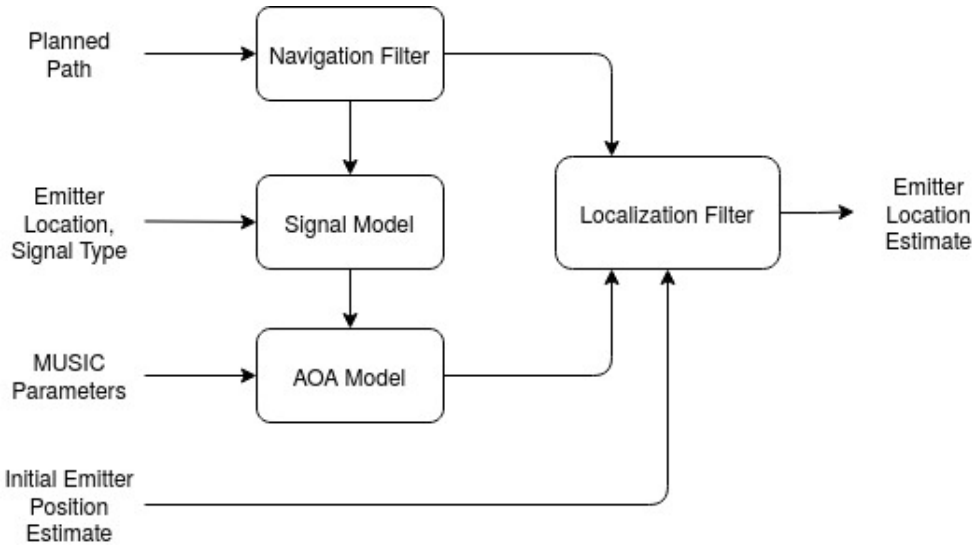

Figure 5.4: Information flow for HWIL system

Each component operated within a networked ROS environment to allow timing synchronization among elements as well as the ability to pass information from system to system. The simulation uses pre-recorded data from a tactical grade GPS/INS device to simulate the navigation solution over the simulation time. As the position changes, the difference between the location of the source and the current solution is used to generate a body frame vector for the AOA simulation. The information is then passed to the signal simulation system in the

body-spherical frame to appropriately delay the signal for the receiving USRP. The signal is then appropriately delayed to represent a signal received from the predetermined location to the current location represented by the navigation solution's pose. The attenuation system handles the signal attenuation at integer dB scaling. The remaining fractional dB is handled by software by adding white noise across all samples relative to the power of the received signal. The power and phase appropriate signal samples are passed into the AOA model. The AOA model then computes the music solution based on the parameters and received signals. The estimated AOA is passed into the localization filter along with measurement variance and current navigation solution.

5.2. Signal Calibration

There are two main calibrations required for the signal calibration. The first is a relative power calibration across all antennas receiving the same signal. This calibrates the signal power at the receiving element relative to the reference antenna. The second calibration is a clock calibration that time aligns the four inputs due to the N310 using a signal for each pair of antennas. Correcting these two biases are done at the operation frequency of interest, GPS L1 in this case. This calibration process is done by transmitting a CW tone at the center frequency through the attenuation and phase delay system to the receiving system via RF cabling. At the receiving port, the signal is not perfectly polarized and has phase error in each pair of signals. Figure 5.2 shows an example of an unbalanced IQ before and after balancing for a single antenna.

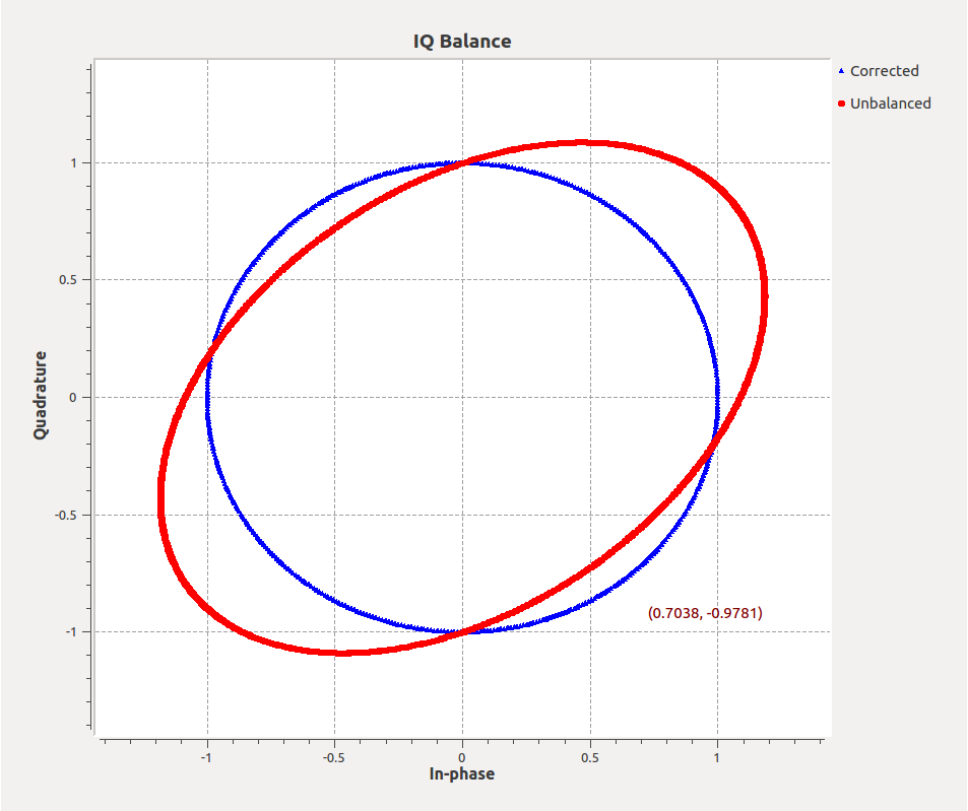

Figure 5.5: IQ Balance correction before and after

The received signal is sampled and used to create an ellipse calibration scaling for the IQ values to correct for the mismatch.

At this point the signals should be adjusted to the correct power relative to the reference antenna. This calibration is used to adjust all samples received for the duration of the system being powered on. Phase coherency is achieved by sampling the same signal and averaging the phase offset between the carrier waves on all antennas. The signals are then corrected by phase as after correcting for the amplitude offsets. Figure 5.2 shows the received carrier wave phase offsets for each of the signals before correction.

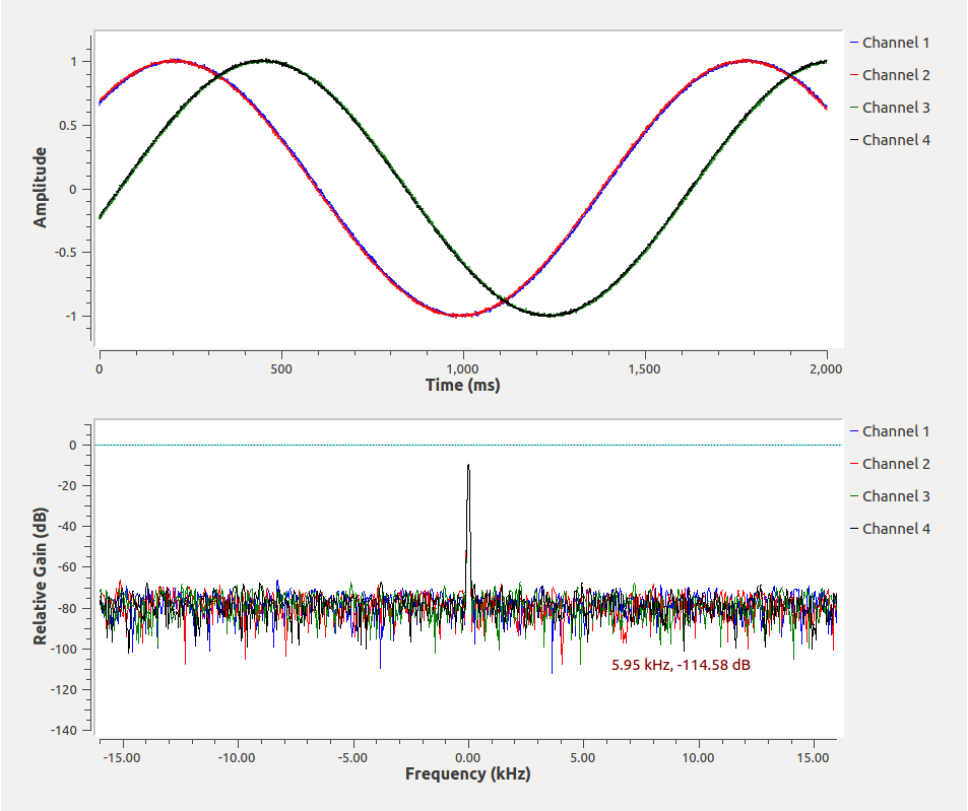

Figure 5.6: Clock error Pre-correction

After the two calibrations, the signals should be nearly identical with the exception of the inherent noise of the front end recording device.

In order to verify the signal is appropriately calibrated, the MUSIC estimation can be ran on the signal that is power and phase calibrated. If the the phase and power calibration are correct, the received signal would not have a phase delay and would be equal in power. In the MUSIC algorithm, an equally delayed signal and equal power signal should produce a peak power at the search space directly over the array. This would be at an elevation of ninety degrees.

To further represent the calibration process for a theorized antenna system, figure 5.7 shows the math behind the calibration process using a CW tone.

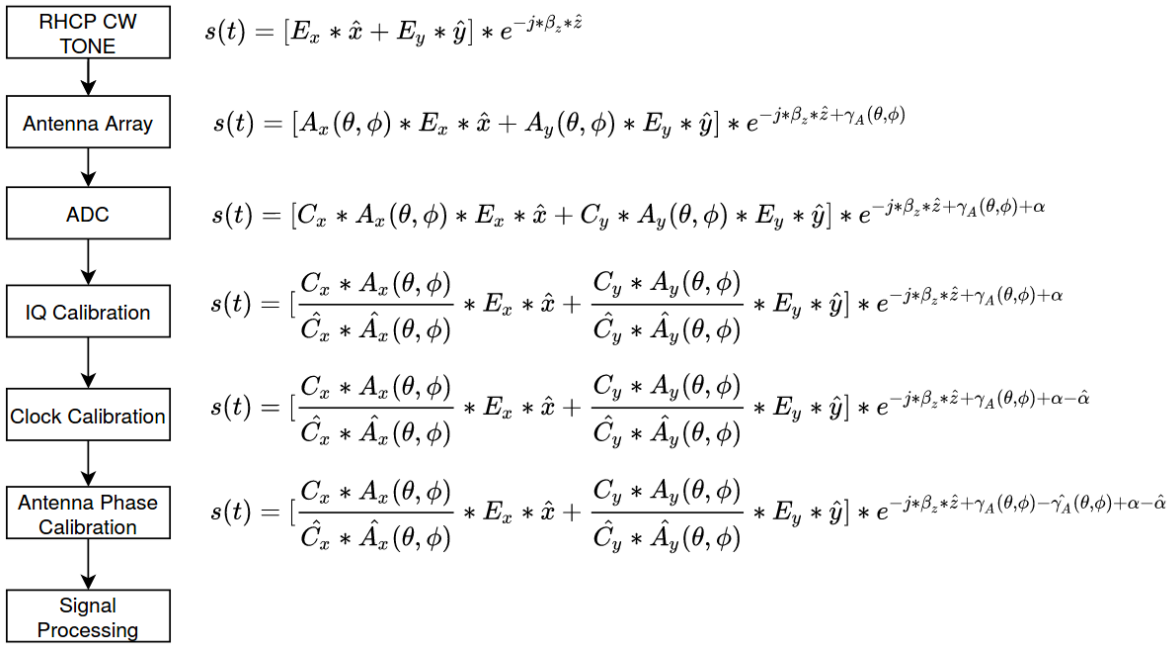

Figure 5.7: Front End Calibration

Refer to table 5.2 for each variable's definition and description.

Table 5.3: Estimation Equation Variables

Equation	**Parameter**	**Description**
All	E_x	Primary axis X direction Electric Field magnitude
All	E_y	Primary axis Y direction Electric Field magnitude
All	$\hat{x}$	Primary axis X direction
All	$\hat{y}$	Primary axis Y direction
All	$\hat{z}$	Primary axis Z direction
All	β_z	Wave propagation constant
Antenna Array	$A_d(\theta, \phi)$	Antenna polarization mismatch constant as a function of θ and ϕ in the direction of d
Antenna Array	$\gamma_A(\theta, \phi)$	Antenna phase shift constant as a function of θ and ϕ for antenna A
ADC	C_d	ADC Gain mismatch ratio from a specific antenna to the datum antenna, this value is one for the datum antenna
ADC	α	ADC phase error from a specific antenna to the datum antenna, this value is zero for the datum antenna
IQ Calibration	$\hat{A}_d(\theta, \phi)$	Estimate of the gain in the direction of the signal based on the antenna manifold in the direction of d
IQ Calibration	$\hat{C}_d$	ADC Gain mismatch ratio from a specific antenna to the datum antenna, this value is one for the datum antenna
Clock Calibration	$\hat{\alpha}$	Phase error shift in samples relative to the datum antenna
Antenna Phase Calibration	$\hat{\gamma_A}(\theta, \phi)$	Estimate of Phase delay caused by the antenna

The signal is represented in the E and H fields as a wave traveling in the $\hat{z}$ direction. Passing through the antenna introduces an antenna gain and phase offset which can be represented as antenna manifold data. The signal is then quantized on the ADC which potentially introduces a small timing error during long sampling periods. The samples are then passed through the IQ calibration and clock(phase) calibrations as shown previously. At this point correcting for the antenna phase differences for each antenna, the samples can then be used in direction finding signal processing algorithms.

5.3. Simulation Signal Generation

The generation of the signal being passed into the music algorithm was done by the collection of hardware from table 5.1. Figure 5.8 shows the different connections required to make the signal generation time and pose appropriate for a source location of choice.

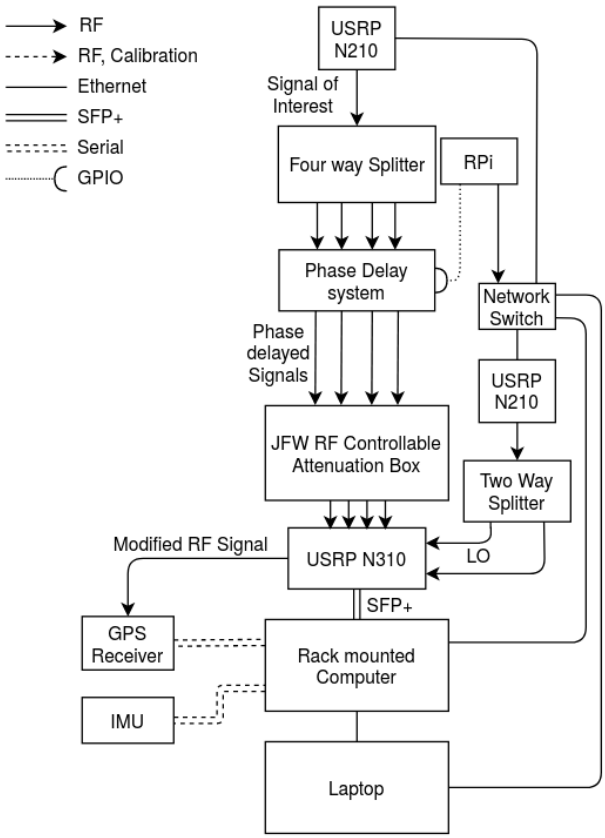

Figure 5.8: HWIL system for simulations

The N210 at the top of the block diagram is the signal generation system. The signal is split four ways and phase delayed according to the current pose of the ROS node replaying the GPS/INS data and the array response. These signals are then passed into the power attenuation system correcting for the expected power levels. Equation 5.3 shows the relationship between the generated signal power and output signal power of the attenuation system.

$$Output_{dBm} = Tx - Splitter_{dB} - DelaySys.Loss_{dB} - Pathloss \tag{5.1}$$

The signals are then passed into the N310 to be multiplied by the calibration parameters estimated in the previous process. Then the signals quantized for each antenna. The signal can then be used to generate the directional measurement. At this point the weighted signal could then been passed to the RF receiver. Due to to the requirement of having the current pose, this portion was not utilized but could be used for other GNSS receivers. The directional measurements were then passed through the asynchronous updates to the ROS node system to be used in various localization methods. In the interest of being able to run multiple localization algorithms, the localization inputs were recorded in the ROS software. Post processing of the system inputs was done in Matlab. While this system produces a power and phase corrected signals from a simulated device, other errors still exist and are not considered such as the clocks in each transmitting device. Although software timing corrections were applied approximately every second, sample to sample errors exist and are unaccounted for which limits high dynamics in this system. Another high frequency operation limitation exists in the phase control system limited by the Raspberry pi's GPIO output rate. Accounting for and providing low phase noise clock inputs to the generation systems as well as the use of a higher data rate on the phase delay system would allow for simulation of relatively high dynamics.

An example of the results of the system described can be seen in the following figures, the position, attitude, and AOA measurements are shown from figures 5.3 to 5.3.

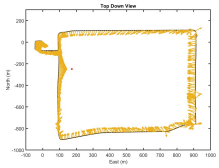

Figure 5.9: Observer Path, Bearing Measurements and Emitter

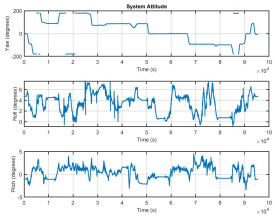

Figure 5.10: Observer Attitude

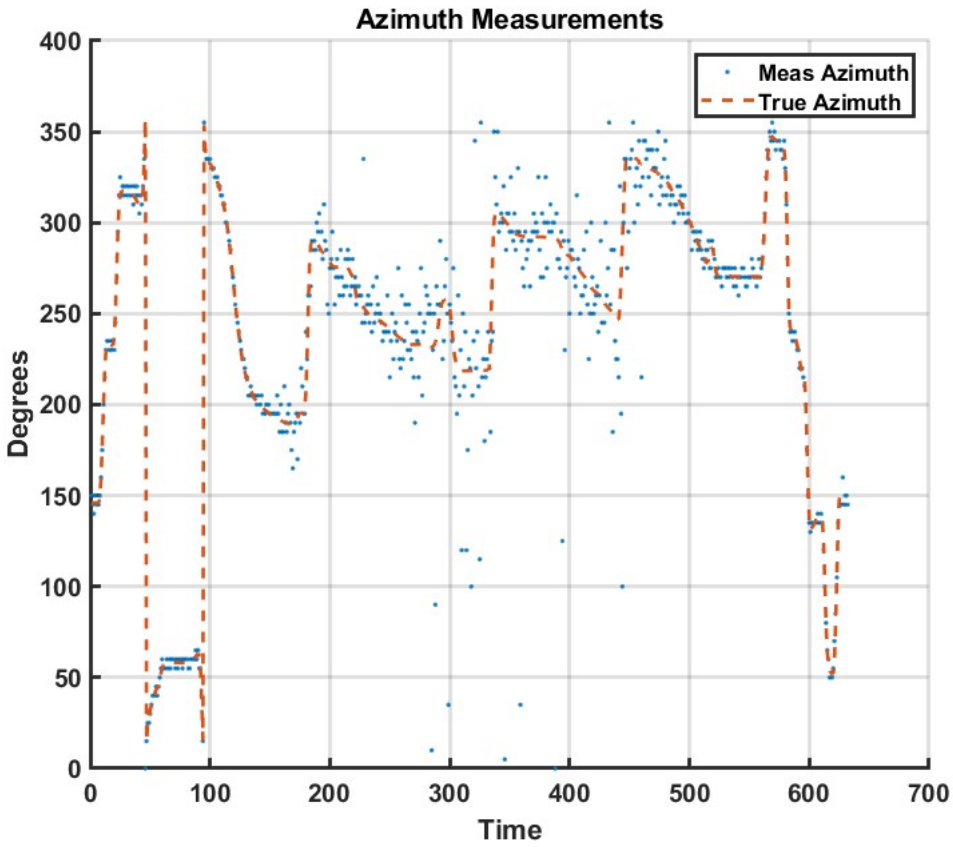

Figure 5.11: Observer Bearing Measurements

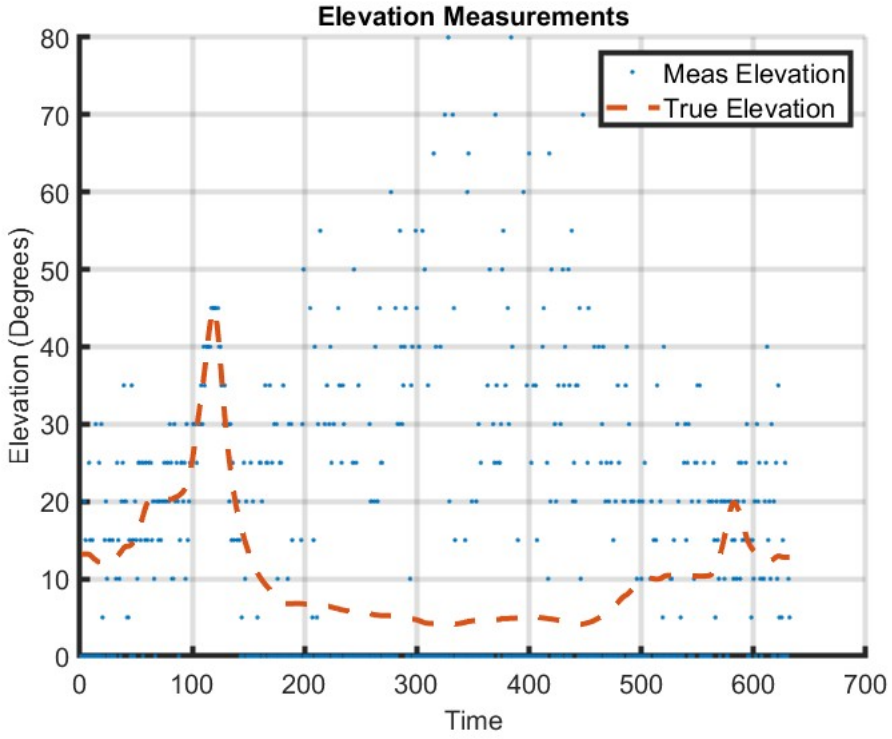

Figure 5.12: Observer Elevation Measurements

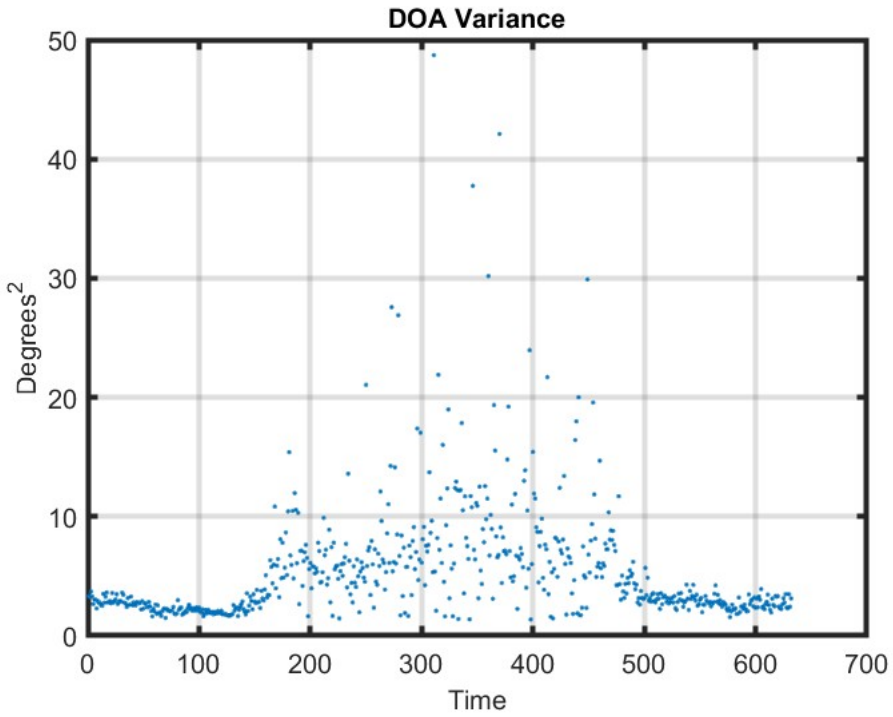

Figure 5.13: Measurement Variance via mapped eigenvalue ratios to Monte Carlo Simulations

Figure 5.3 shows both the path, ideal bearings and position of the source device. In this case the device was chosen at Jordan Hare stadium at a chosen elevation simulating a device at the top of the stadium. This source device is assumed to be a small PPD device at $10dBm$. This allowed the directional estimate variance to grow to a significantly noisy measurement at the ranges experienced. A combination of the measurements taken on this path can estimate the location of the source. This path is derived from measurements taken from a Honeywell E-Talin GPS/INS system that provides the pose information required.

Representing the error of the measurements taken, figures 5.3 and 5.3 show the measurement variance over the duration of the simulation. The discrete steps between the measurements are caused by the MUSIC algorithm due to computation limitations which limit search space resolution to less than infinite. Ideally manifold data which is measured in discrete points would be the limiting factor in the search space. In this case the resolution is limited to five degree increments

The variance of the measurement provided by the AOA sensor is highly non-linear and can be approximated with estimated signal parameters. While this works in some cases such as CW tones, broad band noise signals cen be more difficult to properly estimate. Using the eigenvalues from the MUSIC spectrum provide some insight to the confidence of the spectrum's estimate of direction. Figure 4.3 shows the ratio of the eigenvalues relative to the smallest eigenvalue provided by the decomposition of the covariance matrix. This is directly proportionate to the range and therefore received signal power. Mapping the AOA error to measurement variance through the eigenvalue ratio and known RMS errors as shown in figure 4.3. Different mappings are required for each antenna array, MUSIC signal parameters and receive signal type. Each of these change the MUSIC spectrum error non-linearly.

5.4. Source Location Estimation Models

The two dimensional position estimation is useful for scenarios where the device being localized can be constrained to a plane. To observe the location, the observer needs position, heading and bearing measurements for each measurement time. Considering the case where the observation platform and the transmitting device are co-planar, the observation platform can

localize the transmitter with the use of two independent measurements from different locations. Figure 5.4 shows a case representing this noiseless AOA scenario from three locations. The two unknowns, x and y source positions, can be solved for directly with two measurements.

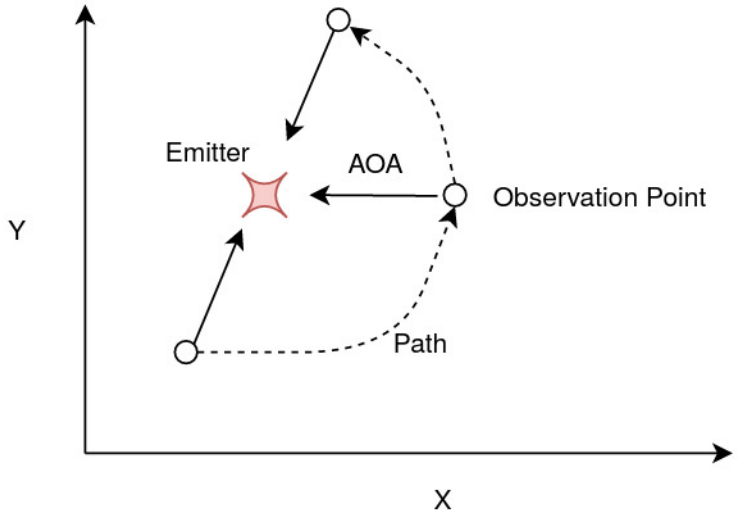

Figure 5.14: Example of planar triangulation

As the number and diversity of measurements increase, the resultant solution should become more accurate.

5.4.1. Non-Stochastic Models

The non-stochastic models do not utilize methodologies to capture the information about the measurement confidence. Due to the non-linearity, difficulty in accurate modeling and unknown signal environment, measurement variance estimates can suffer dramatically under certain conditions. For this reason, the non-stochastic estimates can be used as both an initialization as well as an averaged intersection over a windowed group of measurements. These are expected to perform poorly in comparison to the continuous estimation methods. Utilizing geometric formulas such as centroids and triangle incenters for triangulation of three or more measurements provides instantaneous solutions but are computationally heavy when a very large number of measurement permutations are iterated over. To represent the geometric solutions, figure 5.4.1 shows the physical representation for the centroid calculated with noisy directional bearing measurements.

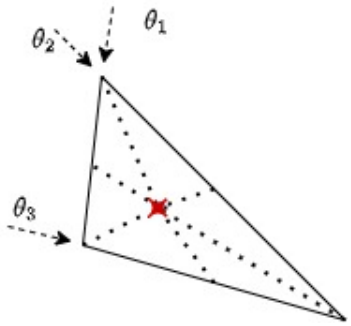

Figure 5.15: Instance of centroid triangulation

While being purely geometric, it can produce adequate solutions at a single time point but requires sufficient angular diversity to create an enclosed area that sufficiently represents the solution. While this type of solution can be useful for intermittent observations of a signal, it does not provide the same quality solution as stochastic estimations. The solution uses line intersections of the three measurements used, then taking the mean of the intersections A, B and C. The incenter method shown in 5.4.1 uses a similar method but splits the angle and uses basic trigonometry to solve for the center point.

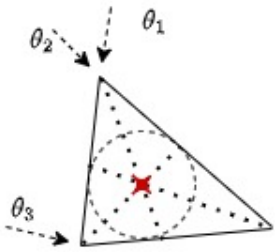

Figure 5.16: Instance of bisector triangulation

The incenter is the another averaging method but is weighted by the side lengths a, b and c. These solution works well in unbiased, low noise scenarios but would suffer from a single noisy measurement. The mathematical representation of these methods are seen in Equations 5.2 and 5.3

$$Centroid = [\frac{A_x + B_x + C_x}{3}, \frac{A_y + B_y + C_y}{3}] \tag{5.2}$$

$$Incenter = [\frac{a * A_x + b * B_x + c * C_x}{a + b + c}, \frac{a * A_y + b * B_y + c * C_y}{a + b + c}] \tag{5.3}$$

While these have no considerations for the noise or filtered solutions, they are important methods in initialization. Using these initial estimates of a location is useful in initially avoiding local minimums and are not computationally heavy in comparison to an iterative method for many measurements. These methods were found to be slightly more robust with smaller angular excitation and low measurement counts but more limited than other options with significant measurement noise and numerous measurements.

Beginning with a rudimentary two dimensional solution in Equation 5.4, the measurement model is based purely on the geometric relationship but can be easily extended into various estimation methods.

$$\hat{y} = \tan^{-1}\left(\frac{Y_{emitter} - Y_{receiver}}{X_{emitter} - X_{receiver}}\right) \tag{5.4}$$

The measurements are assumed to be normally distributed as shown in the measurement process, Equation 5.5.

$$\tilde{y} = p(x) + \eta(0, \sigma^2) \tag{5.5}$$

The bearing measurement noise is dependent on many different parameters when generated using a subspace based approach as shown previously in table 4.2 but are treated as Gaussian. The measurement noise is generally zero mean and normal if they are sufficiently small (i.e. high signal power). This assumption breaks down when higher measurement noise is present[32](i.e. Low signal power).

Batch processing can be used effectively but suffers due to the non-linearity of the model which impacts observability in the presence of high noise measurements. Continuing to only utilize bearing measurements, equations 5.5, 5.4 and 5.6 defines a two dimensional source measurement model.

$$\hat{x} = (H^T * H)^{-1} * H * \Delta Y \tag{5.6}$$

This measurement is compared with a Cartesian vector between the estimated position and observation position. to create the estimated measurement. This model can be expanded into the three dimensional form as shown in Equation 5.7 where θ is the azimuth and ϕ is the elevation.

$$\begin{bmatrix} \hat{\theta} \\ \hat{\phi} \end{bmatrix} = \begin{bmatrix} \tan^{-1}\left(\frac{\hat{Y_{emitter}} - Y_{receiver}}{\hat{X_{emitter}} - X_{receiver}}\right) \\ \tan^{-1}\left(\frac{\hat{z_{emitter}} - z_{receiver}}{\sqrt{(\hat{x_{emitter}} - x_{receiver})^2 + (\hat{y_{emitter}} - y_{receiver})^2}}\right) \end{bmatrix} \tag{5.7}$$

Attempting to linearize the model shown in 5.7 produces a model that is marginally stable. If the measurement model is rearranged to accommodate for a different approach, a more stable result can be found in [39]. Redefining tan to $sin * cos^-1$ allows the terms to be isolated and reduced to the standard least squares model. From here the least squares solution can be used for estimates for every new measurement. This solution was found independently of the original solution in [39]. Equation 5.8 shows the same model as derived from [39]

$$X_{emitter} * sin(\theta_i) - Y_{emitter} * cos(\theta_i) = X_{i,receiver} * sin(\theta_i) - Y_{i,receiver} * cos(\theta_i) \tag{5.8}$$

These estimation models are sufficient when sufficient measurements are provided but become unstable without observability. Observability is directly impacted in the same way GDOP is impacted by satellite position diversity, however the metric for localization is not as simple to calculate due to the unknown position of the source. Geometric position measurement combinations that are not conducive to the estimation can cause large errors in a single direction. This is easily seen by the estimation solutions in the early steps with low observability. This should be considered when measurement positions (observer path) can be chosen. The path traveled is important to both minimize time required and error in estimation from a single observer.

Building on similar methods as shown in the least squares solution an extended kalman filter implementation can be created. Equations 5.9 through 5.13 define the estimator.

$$\begin{bmatrix} X \\ Y \\ Z \end{bmatrix} = I_{3x3} + \begin{bmatrix} -V_x \\ -V_y \\ -V_z \end{bmatrix} * dt \tag{5.9}$$

$$H = tan^{-}1(\frac{Y_{emitter} - Y_{Observer}}{X_{emitter} - X_{Observer}}) \tag{5.10}$$

$$K = P^{-} * H * (H * P^{-} * H^{T} + R)^{-1} \tag{5.11}$$

$$P^{+} = (I_{3x3} - K * H) * P \tag{5.12}$$

$$\bar{X_{t+1}} = \bar{X_t} + K * Y \tag{5.13}$$

This implementation utilizes grouped measurements to estimate the position of the emitter. While this implementation is not idealized for this approach, it avoids the problem of range observability. The range observability problem can be addressed with the utilization of a state by state range parameterization and tracking multiple filters to ensure a stable solution is always provided. This problem is discussed at length in several documents focused on radar based applications but originally in [31].

This implementation works sufficiently well for simple low dynamics but suffers in the event of dynamics due to the relative velocity not being modeled. Since the signal cannot be clearly defined in all cases, the instantaneous relative velocity is not observable directly through frequency estimations. This form of the kalman filter was found to marginally stable due to the observability issue with the range estimation. The local minima problem where the solution falsely converges to a location is the primary driver of initial instability. Further work is required to fully define the minimum initialization error to guarantee stability.

Regressing in Bayesian theory to a maximum likelihood estimator allows a search space to be used which does not suffer as much as other methods to the local minima problem given

a sufficient cost function. The maximum likelihood estimator is derived and defined in [41, 32]. The likelihood cost function is given by the difference between the measured AOA and AOA estimate based on the current estimated location. Using the equation shown in 5.14, the liklihood estimate can be accumulated as measurements are provided.

$$J = 0.5 * (\tilde{\psi} - \hat{\psi}) * C^{-1} * (\tilde{\psi} - \hat{\psi}) \tag{5.14}$$

Each of the solutions up to this point are increasing in general complexity and computation requirements. Each implementation is heavily dependent on measurement diversity as well as the measurement variance. The variance is dependent on the signal environment. In an attempt to mitigate the filter's weakness to measurement diversity in a single time point, the filter design needs to change to accommodate a 'tightly coupled' filter state where the measurement is the state.

The assumption of bearing only is still held through each of these implementations. Implementing the angular measurement in a particle filter can help mitigate the lack of range measurement while also estimating only the angle to the emitter with a sufficient number of particles and re-sampling method. The particle filter does not provide any greater observability into the range but does provide multiple instances of solutions that can iterated through measurements to isolate surviving particles.

To define the particle filter, the pseudocode in algorithm 5.4.1 describes the process used in the particle filter implementation. The first step in the filter is to create an initial set of particles that are all equally weighted and evenly distributed over an initial guess area. As directional measurements are provided from the MUSIC algorithm, the particle angles are propagated in the body frame of the observer based on the navigation measurements provided by the GPS/INS system. Comparing these particles to the MUSIC estimate, produces an error using the arc angle between the two points. Equation 5.15 mathematically represents the angle between two points on a unit sphere.

$$\epsilon = \arccos(\sin\phi_1 \sin\phi_2 + \cos\phi_1 \cos\phi_2 \cos\Delta\theta) \tag{5.15}$$

This angle is physically represented in figure 5.4.1.

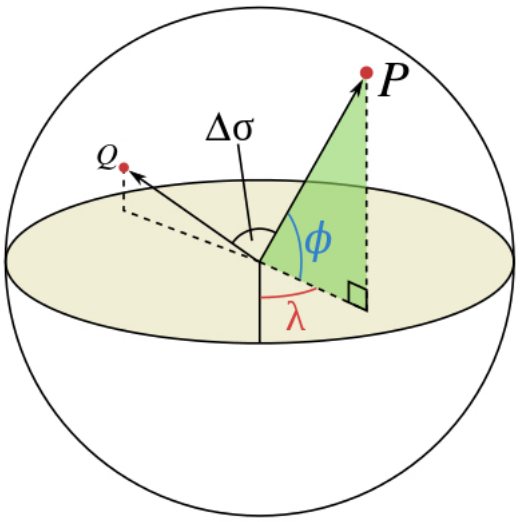

Figure 5.17: Angular Error Representation on a unit sphere

Using this angular measurement, error of the particle is weighted by multiplying the current weight by the arc angle and Gaussian probability density function inverse.

After normalizing the weights, the weights (and particles) that are below one quarter of the maximum weight are dropped. Re-sampling is done by initializing new particles at the weighted average of the current particles. The filter's re-sampling method is done when the filter drops below 80% of its maximum particles. This re-sampling method can be further optimized but is not a concern for processing systems capable of handing this number of particles.

5.5. Results

RMS of the states estimated are used as the comparison between each system. To maintain equal comparisons, the measurements of the sensors remained the same for each system. While the different methods suffer for different reasons, each method still provides something slightly different in different cases. Purely geometric solutions allow instantaneous solutions with little computation. While this is useful for extremely intermittent measurements, these type of approaches suffer from biased or noisy measurements. The continuous methods suffer from observability issues and require noise models but are more robust to noise. Methods

Algorithm 1 Particle Filter - Gaussian Error weighting

Require: $ValidParticles \geq MaxParticles * 80\%$

Require: *Initialized Uniform weight distribution (No prior knowledge of source)*

while Signal Detected **do**

Propagate expected DOAs for each particle

for all Particles (i) **do**

$\hat{P}_i = \hat{P}_{i-1} + f(V_x, V_y, V_z, dt)$

end for

Evaluate particle error

for all combinations of Particles (i) and Measurements (j) **do**

Measured Error

$\epsilon_i = \arccos(\sin\phi_1 \sin\phi_2 + \cos\phi_1 \cos\phi_2 \cos\Delta\theta)$

Weighting Definition

$w_i = w_{i-1} * \epsilon * \frac{1}{GaussianPDF(\sigma^2_{DOA})}$

if $w_i \geq 25\%$ **then**

Drop related particle to weight

end if

Normalize all weights

end for

if $ValidParticles \leq MaxParticles * 80\%$ **then**

Resample Particles around weighted particle average

$NumberNewParticles = MaxParticles - ValidParticles$

$NewParticles = \eta(WeightedAvg, StandardDeviationofremainingParticles)$

$NewWeights = \sum_{n=0}^{I} \frac{w_i}{ValidParticles}$

Normalize weights including new weights

end if

end while

implementing a search space or brute force approaches such as particle filters are better suited for these types of problems but are very heavy computationally. The particle filter and the maximum likelihood estimator have better solutions because they do not suffer from the same limitations. The limitations are due to local minimums and lack of range observability. The range observability can be overcome by parameterization of the states of the continuous filters by the range. This method is shown in **??**. Figures 5.5 through 5.5 show the various estimates and the related errors.

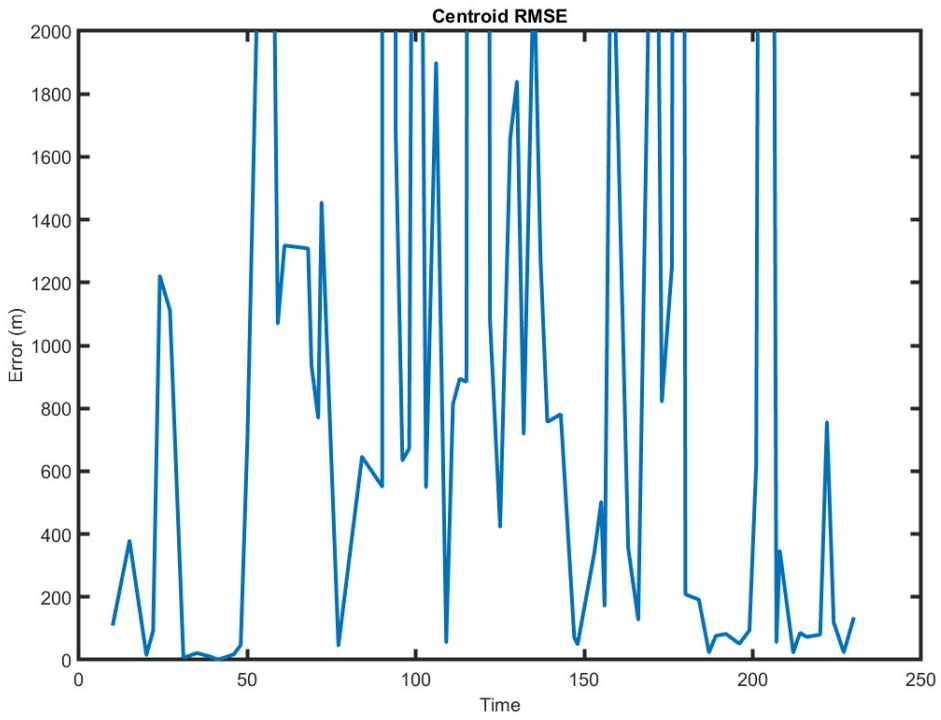

Figure 5.18: Centroid estimate error during the simulation

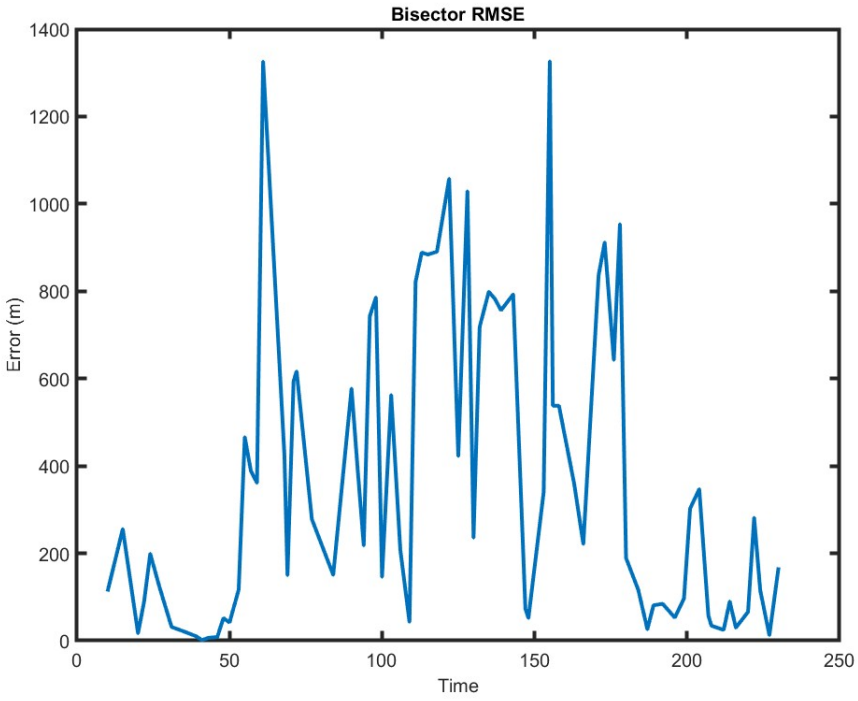

Figure 5.19: Bisector estimate error during the simulation

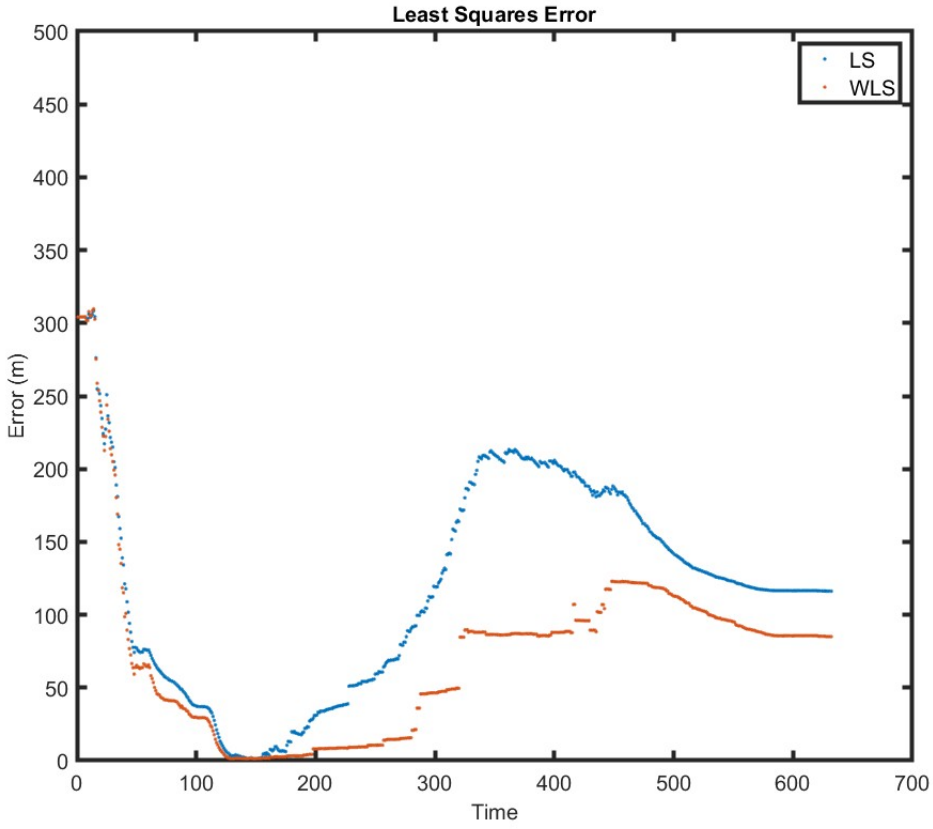

Figure 5.20: Least Squares estimate error during the simulation

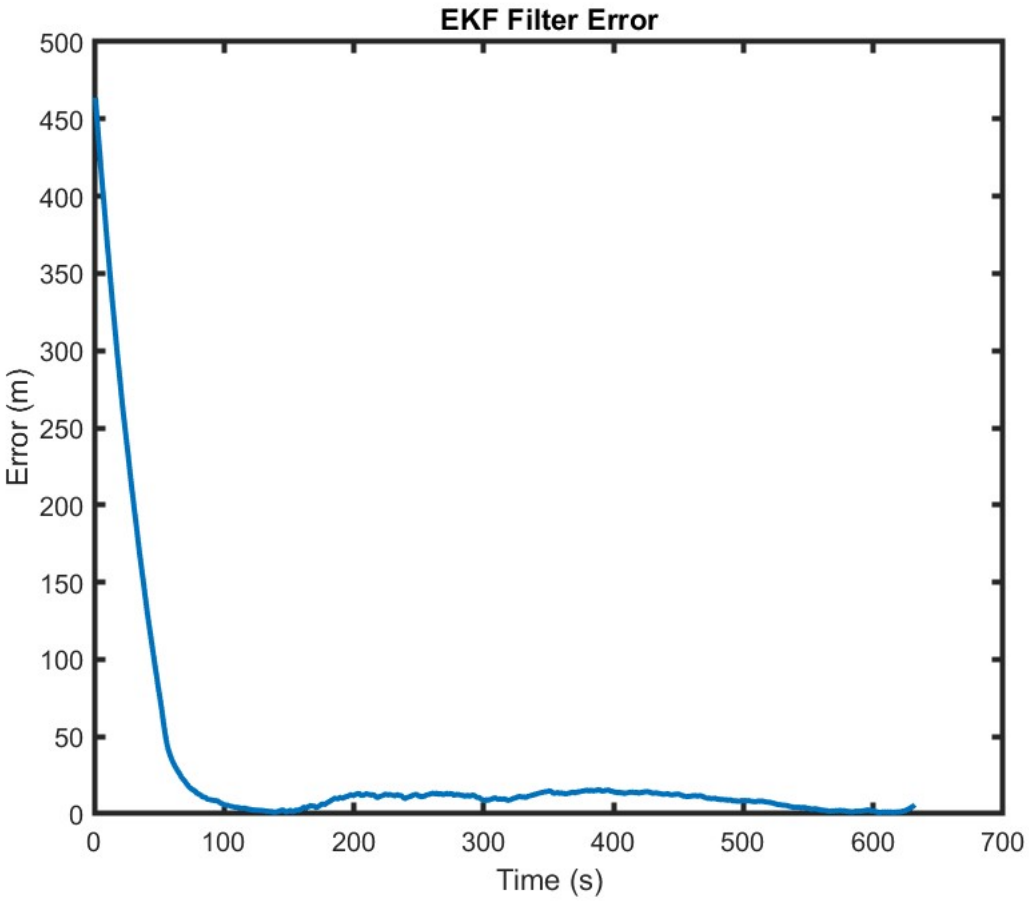

Figure 5.21: Extended Kalman Filter Error during the simulation

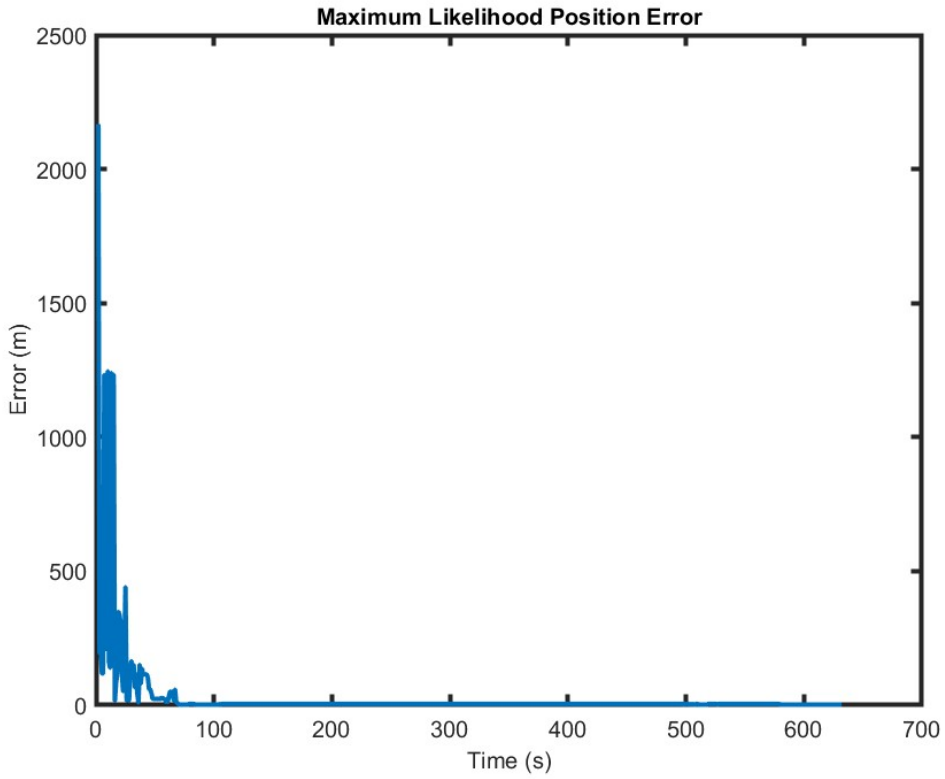

Figure 5.22: Maximum Likelihood Error during the simulation

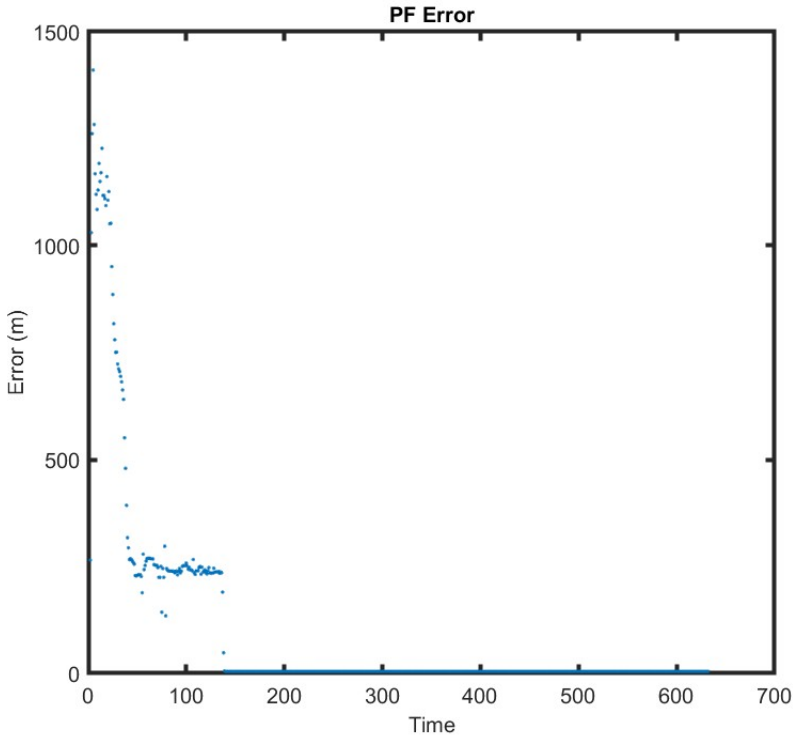

Figure 5.23: Particle Filter Error during the simulation

All systems that require an initial guess are initialized randomly one thousand meters in any direction from the true location. As expected, the geometric solutions suffer from a single noisy measurement which can be seen in figures 5.5 and 5.5. As long as large enough sensor excitation is available the measurements do not intersect near the point of observation. The interaction between the sensor excitation, signal power and measurement variance is highly variable and would require knowledge of the transmitter. To limit the variables, the sensor variance model at the edge of observability suggests a measurement variance of approximately ten degrees. Using this as the limitation for the sensor excitation for all of the results provides a reduction in error spikes for grouped measurements.

The kalman filter result which utilizes grouped measurements provide a sufficiently accurate solution but can still be improved upon in comparison to the heavy computational methods. The maximum likelihood and particle filter results can be improved upon by utilizing additional resources but still provide greater accuracy than the kalman filter. Figures 5.5 and 5.5 show two

instances in time of the estimates of the search spaces and the particles at the shortest distance to the emitter.

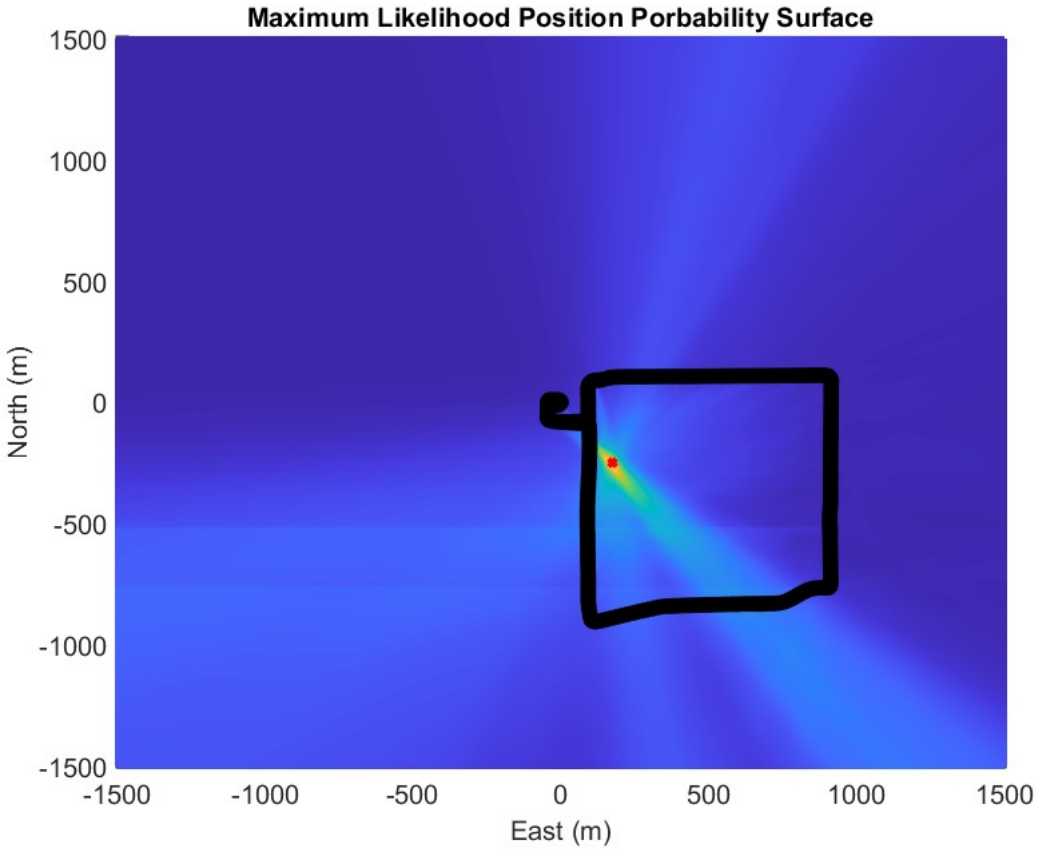

Figure 5.24: Maximum likelihood probability over the estimation area

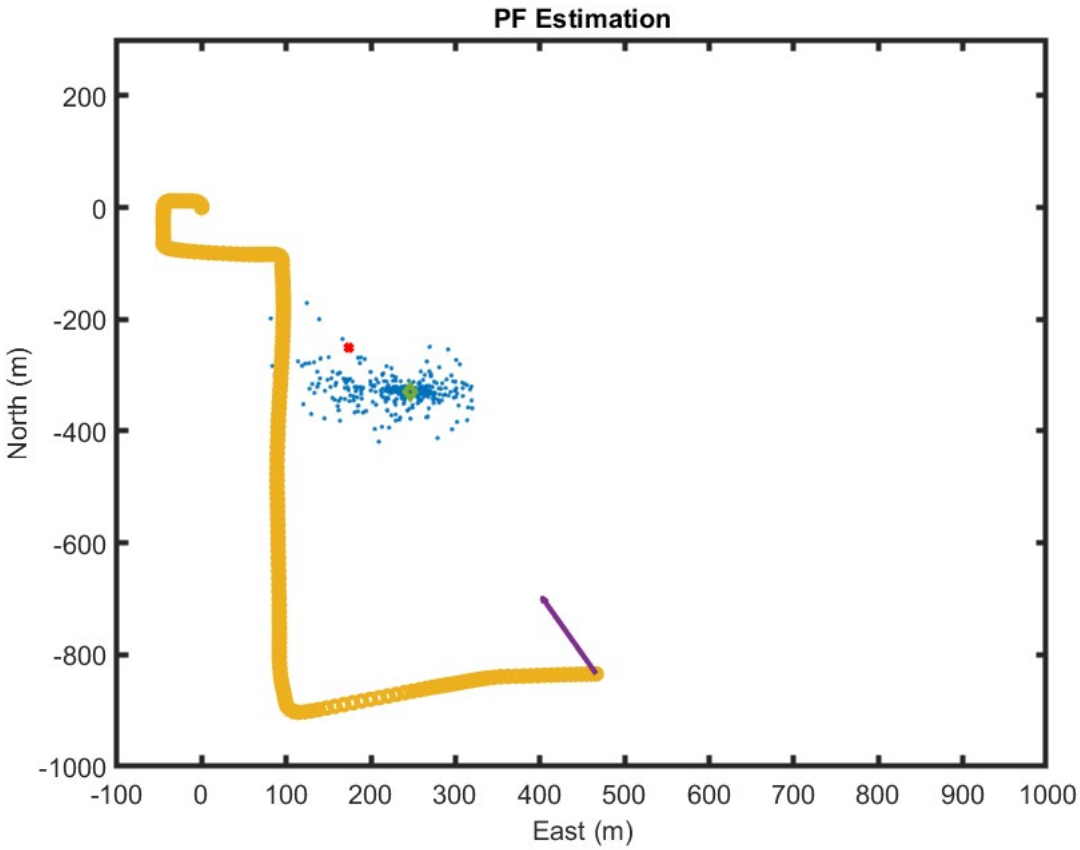

Figure 5.25: Particle distribution over the estimation area

Since they both utilize normal distributions, they show similar results for distribution of solutions.

Chapter 6 Conclusions

The localization of signal's origin can be achieved via several methods from a single observer platform with on board computation. These methods all utilize the same information, including system pose and signal bearings, provided by the platform's systems. The methods have traits unique to each method while they also have limitations due to several different reasons. While the geometric only solutions provide benefits such as low computational cost, initialization for filters and validity checks various estimates, the stochastic filters are capable of providing a better solution at the cost of computation power. These filters can fail in a couple different modes as the localization problem suffers from a few various problems. Systems can fall into a local minimum. These local minimums create false positive solutions and can be seen at various points throughout the search space methods. The other main problem, that drives the choice of estimation solutions, is range to the source is not observable. Without knowledge of the transmitter power, waveform, antenna, direction, surrounding terrain at both locations, and frequency of operation, a power measurement at the receiver cannot be sufficiently utilized.

The search space methods are the most robust and show the greatest accuracy of the estimation methods as well as the most robust methods. Other optimization such as a dynamic search grids for the maximum likelihood could show greater accuracy allowing greater resolution. Additionally the weightings based on different probability distributions that more accurately represent the AOA measurements could provide more accurate estimates as well.

The main limitation of the implementation of the data generation system is the lack of antenna manifold data. The manifold data, which captures the non-linear coloring of the signal power and phase for each antenna, direction and frequency, is not injected as a source of error in the measurements. AOA measurements are impacted by the array's manifold significantly and should be considered. Injection of the manifold data into the signal generation portion by digitally attenuating and delaying signals appropriately before reaching the receiving device

would make the simulation more realistic but would require having that data collected from an appropriate anechoic chamber.

Another limitation of the simulation system is the lack of navigation degradation. While this can be simulated at the signal level, it is difficult to accurately represent the beamforming capabilities of an array. This is mainly due to the manifold data and its related characteristics. The complexity of the simulation representing this type of signal system is dependent on many different variables from navigation to body occlusion.

Directions for future work should include the addition of manifold data into simulation as well as hardware operations. Further signal modeling and simulation should be completed for the monte carlo results for the aoa systems. Characterization of various signals over all directions for a manifold would assist in understanding the impact of each of the signals in relation to the AOA accuracy and resultant beamforming capabilities in relation to those signals. This leads into the concept of ”cross-eyed” jamming. The impact of this type of signal would be interesting on the aoa method as well as what it would take for the array to be able to adequately survive and localize a signal. It is not beyond consideration for a signal system utilizing vision systems along with directional antennas to target a specific device from multiple locations.

Chapter 7　Appendix

This section outlines related information and information that can be utilized to aid in understanding of the concepts presented in the body.

Bibliography

[1] Pseudorandom noise code assignments, 2021.

[2] Poincaré sphere, 2022.

[3] Superheterodyne receiver, Oct 2022.

[4] Fawwaz Alsubaie. Multiple Signal Classification for Determining Direction of Arrival of Frequency Hopping Spread Spectrum Signals. page 75.

[5] H Alemi Ardakani and T J Bridges. Review of the 3-2-1 euler angles: a yaw–pitch–roll sequence. page 9.

[6] John W. Betz. *Engineering satellite-based navigation and timing : global navigation satellite systems, signals, and receivers*. Wiley : IEEE, 2016.

[7] Thomas L Bitner. Detection and removal of erroneous gps signals using angle of arrival. page 103, 2018.

[8] K. Borre, D.m. Akos, N. Bertelsen, P. Rinder, and S.h. Jensen. *A Software-Defined GPS and Galileo Receiver: A Single-Frequency Approach*. Applied and Numerical Harmonic Analysis. Birkhäuser Boston, 2007.

[9] Nathaniel R. Carson, David M. Bevly, Dan B. Marghitu, and Andrew J. Sinclair. *Enhancement and Defense of GPS Navigation Using Signal Processing Techniques. [electronic resource].* 2018.

[10] Patrick Carter. Baseline impact on geolocation. pages 2588–2597, 09 2019.

[11] Howard Chen. The effects of movement speeds and magnetic disturbance on inertial measurement unit accuracy: the implications of sensor fusion algorithms in occupational ergonomics applications. page 109, 2017.

[12] Zhizhang Chen, Gopal Gokeda, and Yiqiang Yu. *Introduction to Direction-of-Arrival Estimation*. Artech House, 2010.

[13] Jianhua Cheng, Jing Wang, and Lin Zhao. A direct attitude determination approach based on gps double-difference carrier phase measurements. *Journal of Applied Mathematics*, 2014:1–6, 2014.

[14] Mahashreveta Choudhary. What are the various gnss systems? *Geospatial World*, Nov 2019.

[15] Pawan Dahiya, Rajesh Mishra, and Rekha Yadav. Design of combined mixer if filter for low voltage and low power automotive radar application. 21, 01 2018.

[16] W De Wilde. The chirp jammer: a gps hit and run, 2020.

[17] Anthony Flores. Navstar gps space segment/navigation user interfaces. Technical report, PNT Capability Area Integration, Portfolio Architect Space and Missile Systems Center, LAAFB, 2021.

[18] Inside Gnss. Fcc fines operator of gps jammer that affected newark airport gbas, Jun 2018.

[19] Frank Gustrau and Dirk Manteuffel. *EM Modeling of Antennas and RF Components for Wireless Communication Systems*. 01 2006.

[20] Sean Victor Hum. Noise in radio systems. Technical report, Toronto University, August 2018.

[21] Tony Jasumback. Gps evaluation: West coast test site.

[22] Claude Jauffret, D. Pillon, and A.-c Pérez-pignol. Bearings-only tma without observer maneuver, 01 2008.

[23] Edward C. Jordan and Keith Balmain. *Electromagnetic waves and radiating systems*. Prentice-Hall of India, 2008.

[24] B. Kim and Mikhail Tinin. Effect of ionospheric irregularities on accuracy of dual-frequency gps systems. *Geomagnetism and Aeronomy*, 47:238–243, 01 2007.

[25] Tony Lacey. Tutorial: The Kalman Filter. page 8.

[26] Sherman Lo, Yu Chen, Fabian Rothmaier, Godwin Zhang, and Chiawei Lee. Developing a dual polarization antenna (dpa) for high dynamic applications. pages 1001–1020, 02 2020.

[27] Sherman Lo, Yu Hsuan Chen, Hridayangam Jain, and Per Enge. Robust GNSS Spoof Detection using Direction of Arrival: Methods and Practice. pages 2891–2906, Miami, Florida, October 2018.

[28] Gang Lu. Development of a GPS Multi-Antenna System for Attitude Determination. page 195.

[29] Scott M Martin. Closely Coupled GPS/INS Relative Positioning For Automated Vehicle Convoys. page 117.

[30] P. Misra and P. Enge. *Global Positioning System: Signals, Measurements, and Performance*. Ganga-Jamuna Press, 2011.

[31] Steven C. Nardone and Vincent J. Aidala. Observability criteria for bearings-only target motion analysis. *IEEE Transactions on Aerospace and Electronic Systems*, AES-17:162–166, 1981.

[32] N. O'donoughue. *Emitter Detection and Geolocation for Electronic Warfare*. Artech House electronic warfare library. Artech House, 2019.

[33] Richard Parker, Karen Bayne, and Peter Clinton. Robotics in forestry. *New Zealand Journal of Forestry*, 60:8–14, 02 2016.

[34] B.w. Parkinson and J.j. Spilker. *Progress In Astronautics and Aeronautics: Global Positioning System: Theory and Applications*. Geografia (E-libro). American Institute of Aeronautics & Astronautics, 1996.

[35] B.w. Parkinson, J.j. Spilker, S.u.j.s.b. Parkinson, P. Axelrad, and P. Enge. *Global Positioning System: Theory and Applications*. Global Positioning System. American Institute of Aeronautics and Astronautics, 1996.

[36] Ling Pei, Jingbin Liu, Robert Guinness, Yuwei Chen, Tuomo Kroger, Ruizhi Chen, and Liang Chen. The evaluation of wifi positioning in a bluetooth and wifi coexistence environment. pages 1–6, 10 2012.

[37] R.a. Poisel. *Modern Communication Jamming Principles and Techniques*. Artech House.

[38] Caroline Rees. Sigint technology to help expand gray eagle, May 2015.

[39] Robert G. Stansfield. Statistical theory of d.f. fixing. *Journal of the Institution of Electrical Engineers - Part IIIA: Radiocommunication*, 94:762–770, 1947.

[40] Joshua Starling and David M. Bevly. *Error Analysis of Carrier Phase Positioning Using Controlled Reception Pattern Antenna Arrays. [electronic resource].* 2017.

[41] R.f. Stengel. *Optimal Control and Estimation*. Dover books on advanced mathematics. Dover Publications, 1994.

[42] William Tewelow. The evolution of gps satellites and their use today, Oct 2020.

[43] Michael P. Vitus. Carrier phase techniques. Technical report, Stanford, August 2005.

[44] Tanner Watts, Scott Martin, and David Bevly. A GPS and GLONASS L1 Vector Tracking Software-Defined Receiver. pages 162–176, Reston, Virginia, February 2019.

[45] Joshua Wood. Detection of gnss faults using receiver clock drift estimates. page 242, 2020.